THESIS FOR THE DEGREE OF DOCTOR OF PHILOSOPHY

LONGITUDINAL FORCE DISTRIBUTION AND ROAD VEHICLE HANDLING

by

MATTHIJS KLOMP

Department of Applied Mechanics
CHALMERS UNIVERSITY OF TECHNOLOGY
Gothenburg, Sweden, 2010

Longitudinal Force Distribution and Road Vehicle Handling

MATTHIJS KLOMP

ISBN 978-91-7385-391-0

Doktorsavhandlingar vid Chalmers tekniska hï¿½gskola
Ny serie Nr 3072
ISSN 0346-718X

Department of Applied Mechanics
Chalmers University of Technology
SE–412 96 Gothenburg
Sweden
Telephone: +46 (0)31–772 1000

Chalmers Reproservice
Gothenburg, Sweden 2010

To Sara

Longitudinal Force Distribution and Road Vehicle Handling

MATTHIJS KLOMP
Department of Applied Mechanics
Chalmers University of Technology

Abstract

The distribution of longitudinal forces has a large influence on vehicle handling characteristics such as the driver/vehicle interaction, road holding and yaw stability, in particular during combined traction/braking and cornering near the grip limit of the tires. In order to select and develop suitable driveline systems and associated active control that provide consistent driver/vehicle handling, maximum road holding and sufficient yaw stability margins, it is essential to understand the influence of a particular drive force distribution on these handling characteristics. Due to the highly non-linear interaction between the longitudinal and lateral forces near the grip limit, the studies in this area have thus far focused on prototype testing and/or simulations with sophisticated vehicle models. By developing simpler models and more informative graphical representations, the understanding of the fundamental interaction of the drive force distribution and vehicle handling can be further improved and thereby facilitate enhanced development of future driveline systems.

In this thesis, improved graphical representations, simpler models and new approaches to optimization of longitudinal force distribution are presented. These new methods focus particularly on exploring and maximizing the road holding capability of the vehicle. Also, new indicators of a likely loss of yaw stability are presented for one particularly severe driving maneuver. One area of application of the presented optimization methods, is demonstrated for case when the entry speed is too high to track a particular curve due to friction limitations. For this scenario a new parabolic path recovery strategy is developed based on a particle representation. This strategy, when implemented in to the planar motion of a vehicle, is shown to exhibit considerably less deviation from the intended path than currently proposed methods based on yaw moment allocation.

The results obtained in this work are applied for analysis of the performance of a wide range of driveline systems, and are expected to have applications also in the associated active control for these systems. Overall, the present work has expanded the fundamental framework of vehicle modeling, optimization formulations and graphical representations for analysis and optimization of a wide range of driveline system properties and vehicle level characteristics.

Keywords: vehicle dynamics, vehicle handling, combined grip, drive force, longitudinal force distribution, combined slip, quasi steady-state, optimization.

List of publications

This thesis is based on the work contained in the following papers, referred to by Roman numerals in the text:

I. Klomp, M. and Thomson, R., *Influence of Front/Rear Drive Force Distribution on the Lateral Grip and Understeer of All-Wheel Drive Vehicles*, submitted to: International Journal of Vehicle Design, 2010.

II. Klomp, M., *Longitudinal Force Distribution Using Quadratically Constrained Linear Programming*, submitted to: Vehicle System Dynamics – International Journal of Vehicle Mechanics and Mobility, 2010.

III. Duringhof, H.-M., Klomp, M., Trï¿½nnberg, G., and Wolrath, C., *Development and Vehicle Integration of XWD Driveline Technology*, in: Proceedings of the 21st International Symposium on Dynamics of Vehicles on Roads and Tracks (IAVSD 2009), Stockholm, Sweden, 2009. (slightly modified)

IV. Klomp, M., Billberg, J., and Douhan, A., *Driver Warning Strategies for a Critical Cornering Maneuver*, in: Proceedings of the 21st International Symposium on Dynamics of Vehicles on Roads and Tracks (IAVSD 2009), Stockholm, Sweden, 2009. (slightly modified)

V. Klomp, M., Gordon, T. J., Lidberg, M., *Optimal Path Recovery for a Vehicle Tracking a Circular Reference Trajectory*, submitted to: Journal of Dynamic Systems, Measurement, and Control, 2010.

In addition to the papers listed above, this author has also been involved in related work presented in references [4, 8, 28–33, 52, 53].

Author's Contribution to Appended Papers

The individual contribution of this author to the appended papers is such that:

- In Papers I, IV and V this author wrote the main part of the paper and did the mathematical and numerical modeling and performed all numerical simulations.
- Paper II is this author's own work.
- In Paper III this author was responsible for the writing, modeling and simulations presented in Figure 5, Section 3 and 4.1 and performed the dropped-throttle simulations presented in Section 5.2. Additionally, this author contributed to the editing of the overall structure of the paper.

Acknowledgements

This thesis would not have been possible without the help and support of many people around me, to only some of whom it is possible to give particular mention here. Nonetheless, all contributions, small or great, are much appreciated!

Specifically, I wish to thank my supervisors Anders Boström, Bo Egardt, Mathias Lidberg and Robert Thomson from Chalmers and Youssef Ghoneim and Gunnar Olsson at Saab, for providing excellent academic supervision and guidance of this work. In particular to Gunnar and Mathias, for having been an invaluable part of this project from its inception until now. I also want to thank Tim Gordon for supervision of the work presented in Papers II and V.

To those who inspired me to pursue graduate studies, I would like to mention Olof Ekre, Per Nylï¿½n and Kjell Niklasson, in particular. Further, my sincere thanks to Leo Laine; you, as an experienced fellow student, greatly helped and encouraged me during the first crucial years of this project.

This work has been financially supported by Saab Automobile and the Swedish government research program Intelligent Vehicle Safety Systems (IVSS).

I further want to express my gratitude to my dear friends in church, my fellow students at Chalmers and my colleagues at Saab, for inspiration and support. I am also very grateful for the prayers and fellowship with my colleagues in our prayer group at Saab and the heartwarming support we received from the group at Volvo during the turbulent times at Saab last year.

Finally, I want to thank my entire family, my dear parents in particular, for never ending support. Above all, I am deeply grateful for my beloved wife Sara, and our lovely children Lukas, Tobias and Alicia, and for your continuous encouragement and love.

Matthijs Klomp
Gothenburg, June 2010

Nomenclature

The nomenclature used in this work follows ISO standard 8855:1991 [19] for the vehicle dynamics terminology. The indices used are given in Table 1, the Greek variables in Table 2 and the latin variables in Table 3. The acronyms used are summarized in Table 4 and selected terms are explained in Table 5.

Table 1: Indices

Index	**Description**		
0	Static / nominal		
1	Front axle	2	Rear axle
i	Front/Rear index	j	Left/Right index
IN	Input from power source		
st	Single-track	tt	Two-track
lim	Maximum value	ref	Reference or target value
X	Longitudinal, positive forward	Y	Lateral, positive to left
Z	Vertical, positive upward		
$\dot{}$	Derivation with respect to time	$\ddot{}$	Second time derivative

Table 2: Greek variables

Variable	**Unit**	**Description**			
α	[rad]	Tire slip angle	β	[rad]	Body slip angle
δ	[rad]	Wheel steered angle	δ_{H}	[rad]	Steering-wheel angle
ψ	[rad]	Yaw angle	κ	[-]	Longitudinal tire slip
σ	[-]	Combined tire slip	μ	[-]	Friction coefficient.
ξ	[-]	Drive force ratio	χ	[-]	Combined slip factor

Table 3: Latin variables

Variable	Unit	Description			
$\boldsymbol{A}$	n/a	State matrix	$\boldsymbol{a}$	[m/s^2]	Acceleration vector
a	[m/s^2]	Acceleration	b	[m]	Track width
B	n/a	Input matrix	C_α	[N/rad]	Cornering stiffness
F	[N]	Force	g	[m/s^2]	Gravity
K_{US}	[*]	Understeer gradient	M	[Nm]	Moment
l_1	[m]	Front axle to CoM	l_2	[m]	Rear axle to CoM
l	[m]	Wheelbase	k	[m]	Radius of gyration
P	[W]	Power	R	[m]	Cornering radius
h	[m]	Mass center height	$\boldsymbol{u}$	n/a	Input vector
v	[m/s]	Speed	$\boldsymbol{x}$	n/a	State vector

Table 4: Acronyms

ABS	Antilock braking system
TCS	Traction control system
ESC	Electronic stability control
DYC	Direct yaw moment control
AWD	All wheel drive
FWD	Front wheel drive
RWD	Rear wheel drive
LSD	Limited slip differential
eLSD	Electronically controlled LSD
TVD	Torque vectoring differential
EM	Electric motor
ICE	Internal combustion engine
MMM	Milliken Moment Method
QCLP	Quadratically Constrained Linear Programming
QSSA	Quasi steady-state approximation/assumption
CoM	Center of mass

Table 5: Glossary of selected terms

Term	Explanation
Ackermann angle	The wheel base divided by the cornering radius. A neutral steered vehicle only needs to steer the Ackermann angle to achieve a certain cornering radius.
Combined grip	Combined lateral and longitudinal grip.

Table 5: Glossary of selected terms

Term	**Explanation**
Differential	Device that splits the incoming torque with a fixed ratio to each output while allowing an arbitrary speed difference between the outputs.
Driveline	The powertrain excluding the power source (e.g. combustion engine or electric motor).
Dynamic square	Contour plot of constant levels of lateral grip as function of the front and rear longitudinal forces.
Friction	Resistance to shear forces.
Friction circle	Symmetric combined grip.
Handling	Vehicle dynamics characteristics and capabilities of the driver/vehicle/road system.
Handling curve	Slip angle difference versus the lateral acceleration. The slope of the handling curve is the understeer gradient.
Handling diagram	Plot of a handling curve.
Lateral	Left/right.
Lateral grip	Maximum steady-state lateral acceleration capability of a vehicle. Determines the minimum cornering radius for a given speed.
Longitudinal	Front/rear.
Longitudinal grip	Longitudinal force capability.
Magic Formula	One particular tire model.
MMM Diagram	Unbalanced yaw moment versus lateral acceleration.
Neutral steer	Increases in lateral acceleration requires no change in steering angle to maintain the same cornering radius.
Oversteer	Increases in lateral acceleration requires a decrease in steering angle to maintain the same cornering radius.
Phase portrait	Plots of the solutions of a two-degree of freedom dynamic system for different initial conditions.
Pitch	Front/rear rotation
Powertrain	The powertrain is defined as the vehicle propulsion subsystem, from the power source to the driven wheels.
Quasi steady-state	The time derivatives of the states are small or constant.
Rate	Rate of change with respect to time.
Road holding	Maximum combined grip.
Roll	Left/right rotation.

Table 5: Glossary of selected terms

Term	**Explanation**
Yaw stability	Property of planar motion of the vehicle. If stable and the inputs are fixed, the yaw rate converges (reasonably fast) to a constant value after a disturbance or change in the inputs. For yaw stability, this commonly also implies that the body side-slip angle is small and bounded.
Slip	Quantity that relates a free rolling wheel to a wheel that subjected to forces or moments.
Slip angle	Angle of the velocity vector of the wheel relative to the free rolling direction.
Side-slip angle	Angle of the velocity vector of the center of gravity relative to the vehicle longitudinal axis.
Turn-in yaw moment	Yaw moment that increases the absolute value of the yaw rate.
Understeer	Increases in lateral acceleration requires a increase in steering angle to maintain the same cornering radius. Sometimes understeer refers to the understeer gradient.
Understeer gradient	Partial derivative of the front/rear slip angle difference relative to the lateral acceleration. A negative understeer gradient is means oversteer and a zero understeer gradient means neutral steer.
Unbalanced yaw moment	Product of the yaw inertia and the yaw acceleration.
Vertical	Up/down.
Yaw	Rotation in the road plane.
Yaw moment	Moment around the vertical axis.

Table of Contents

Chapter 1

Introduction

The distribution of longitudinal forces has a large influence on vehicle handling characteristics such as the driver/vehicle interaction, road holding and yaw stability, in particular during combined traction/braking and cornering near the tires' grip limit. In order to analyze and develop suitable driveline systems and associated active control that provide consistent driver/vehicle handling, maximum road holding and sufficient yaw stability margins, it is essential to understand the influence of a particular drive force distribution on these handling characteristics. Due to the highly non-linear interaction between the longitudinal and lateral forces near the grip limit, the studies in this area have thus far focused on prototype testing and/or simulations with sophisticated vehicle models. By developing simpler models and more informative graphical representations, the understanding of the fundamental interaction of the drive force distribution and vehicle handling can be further improved and thereby facilitate enhanced development of future driveline systems.

1.1 Background

If driving under challenging road conditions, the driver may become aware of the influence of the drive force distribution on the vehicle handling characteristics. Driving a rear-wheel drive (RWD) vehicle on a slippery surface one may have experienced that the vehicle started to skid sideways when accelerating in a turn. Doing so in a front wheel drive (FWD) vehicle, and the vehicle may turn less than desired, as opposed to too much for the RWD vehicle. Under these challenging conditions a modern all wheel drive (AWD) vehicle provide better road holding when accelerating (traction) than both FWD and RWD vehicles.

Vehicle dynamics is the theory of how tire and aerodynamic forces acting on

a vehicle affect the vehicle motion, response, stability, and other characteristics. Vehicle dynamics thereby provides the framework necessary to understand the phenomena described above and which are important for a safe driver/vehicle/road interaction.

In its infancy, the main focus in the field of vehicle dynamics was on improving the brakes and tires due to the demands of increased vehicle speed. Early developments include preventing the rear wheels from locking prior to the front wheels (a common cause of vehicle instability up to that point) through brake proportioning. AWD vehicles, as shown in Figure 1.1, were introduced as early as 1900 in the Lohner-Porsche electric vehicle and 1903 in the Spyker 60/80 HP racer and AWD-vehicles have gone as far as to the moon! The Lohner-Porsche had in-wheel electric motors as did also the Lunar Rover vehicles used during the Apollo 15, 16 and 17 lunar missions, a technology often seen as the ultimate all-wheel drive technology [5, 17, 23].

Electronic control systems were introduced through anti-lock braking systems (ABS), which prevented the wheels to lock during hard braking and thereby permitting the driver to maintain steer-ability. From ABS systems, traction control systems (TCS) were developed, which prevent wheel spin while accelerating. This electronic control of the brake system eventually lead to electronic stability control (ESC) systems which use autonomous brake intervention to steer the vehicle in a situation when skidding is detected by the system. In its most recent development, vehicle dynamics control has expanded to include active control of steering, driveline, and suspension sub-systems. Among these, this study focuses on the analysis of active all-wheel drive (AWD) systems, which are reaching a point where the longitudinal forces on all four wheels can be independently controlled [46]. With this enhanced capability enabling better safety margins due to an enhanced road holding, and the issues with higher possible cornering speed, this area motivates a considerable amount of research and development activities.

1.2 Motivation

As for the interaction between combined longitudinal and lateral forces, it is well-known that the lateral grip of tires reduces with increased longitudinal forces due to tire/road friction limits [48, 63]. This is often modeled such that the vector sum of the lateral and longitudinal forces must lie within a circle (or ellipse) – the friction circle. Important early contributions to expand the understanding of these effects on a tire level to vehicle level handling characteristics are made in for instance [47] where the influence of longitudinal forces on the lateral grip as well as the understeer of the vehicle is also modeled using the friction circle concept. The lateral grip is important for the cornering capability of the vehicle

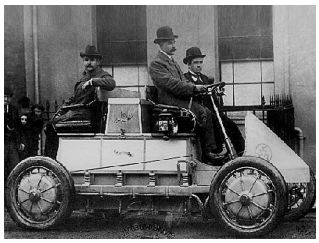

(1900) Lohner Porsche

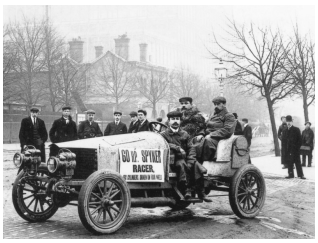

(1903) Spyker 60 HP Racer

(1985) Audi Sport Quattro [62]

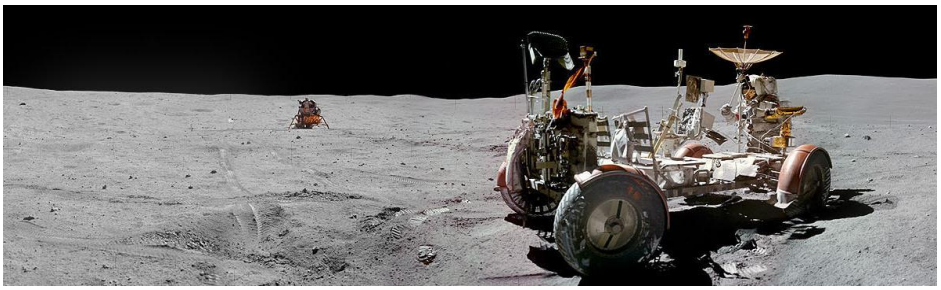

(1972) Apollo 16 Lunar Roving Vehicle with Lunar Module *Orion* in the background. [10]

Figure 1.1: Historic AWD vehicles.

and the understeer is an important handling characteristic since it influences the driver/vehicle interaction. Understeer is also important for the yaw stability when the understeer changes to oversteer, see [3, 15, 24, 47, 48] for instance.

Apart from the above studies, regarding the influence of the longitudinal force distribution on the lateral grip or understeer, there are studies of the influence of the drive force distribution on the yaw moment potential [57, 58] or the stabilizing yaw moment [61]. In [61] the authors study both the front/rear and left/right distribution and they report that the vehicle can be actively stabilized during deceleration by transferring brake force from the inner wheels to the outer wheels. These studies paved the way for electronic stability control (ESC) systems that are becoming standard on many vehicles [13, 65, 66] and have had a great impact on vehicle safety [36, 42], primarily by avoiding loss of yaw stability during evasive maneuvers. Further, the effects of longitudinal force distribution are studied separately for different actuators in for instance [1, 2, 22, 51, 57, 70] and as an integrated system in [5, 23, 35, 39, 40, 44]. Most of these studies focus on the development of a particular control system and are often applied to evasive maneuvers such as lane-change maneuvers for which stability improvements are shown over passive systems.

In reviewing the above referenced literature it is found that the vehicle/actuator system is often handled as a largely unknown system that is studied by analyzing the effects of certain inputs on the outputs of that system. Although the standard – linear – operating region of the vehicle is well understood, for the non-linear op-

erating region, however, simple models explaining fundamental phenomena are largely missing. Also, many handling evaluation methods are developed for a constant longitudinal speed and are not suitable for studying the effects of parameter changes of interest here, such as total longitudinal force and/or the front/rear or left/right distribution.

1.3 Objectives

The objectives of this study are to gain better understanding and support industrial application of active driveline systems. The first objective is to expand the fundamental understanding of the interaction between the drive force distribution and limit vehicle handling by means of simple, yet meaningful, models and improved graphical representations. This understanding should secondly support the development of actual driveline systems and feed-forward components in the associated active control.

It is suggested that the optimization of idealized driveline systems is important as reference for the development of actual systems. For this reason development of optimization formulations are part of this study.

In order to focus on performance of the vehicle/driveline system, this study is limited to maneuvers where the steering input is prescribed (open-loop control), meaning that any driver dynamics is excluded. Since the intended application of the obtained results are standard passenger vehicles with a relatively low center of gravity, the dynamics which are modeled are those related to planar vehicle motion, meaning that roll, pitch, driveline and wheel dynamics are replaced with quasi steady-state approximations.

1.4 Thesis Outline

The present thesis is a compilation thesis, meaning that it consists of one summarizing part and a second part comprised of the papers that are included. The summarizing part serves as a general overview of the work and intends to place the appended papers in a common context. The main scientific contributions of this work are reported in the appended papers which are submitted for publication in scientific journals or conferences relevant to this field.

Chapter 2

Vehicle Dynamics Modeling

In order to mathematically analyze and/or optimize the vehicle dynamics system, models are necessary. These models should capture the most relevant properties of the system of interest. Further, by necessity, and to make the analysis as clear as possible, proper simplifications are required. In this chapter four different models of the planar vehicle motion are presented and compared. Additionally, the different tire models used in this study are discussed. This chapter is concluded with a presentation of the different components in modern driveline system. The reader may appreciate this driveline presentation as a background to Papers I, II and III appended to this thesis.

2.1 Vehicle Models

Four different vehicle models are used in this study. All are simple models modeling the planar motion of a vehicle. In these models other dynamics such as for instance roll, pitch, wheel rotation, driveline and tire dynamics are not considered. A good discussion on these assumptions is found in [69] where the conclusion is drawn that, for most maneuvers, the non-linear tire characteristics are the most important to consider. The only paper where a more complex vehicle model is used is Paper III.

The vehicle models used in this work use a vehicle fixed coordinate system. The planar motion is then described using the vehicle longitudinal and lateral velocities and the rotational velocity (yaw rate) as state variables. These state variables are denoted v_X, v_Y and $\dot{\psi}$, respectively. Throughout this work, the steering input and the total drive force are assumed given *a priori*, and the study considers the effect of the distribution of this total drive force.

Next, three models will be presented in more detail. These are the two-track

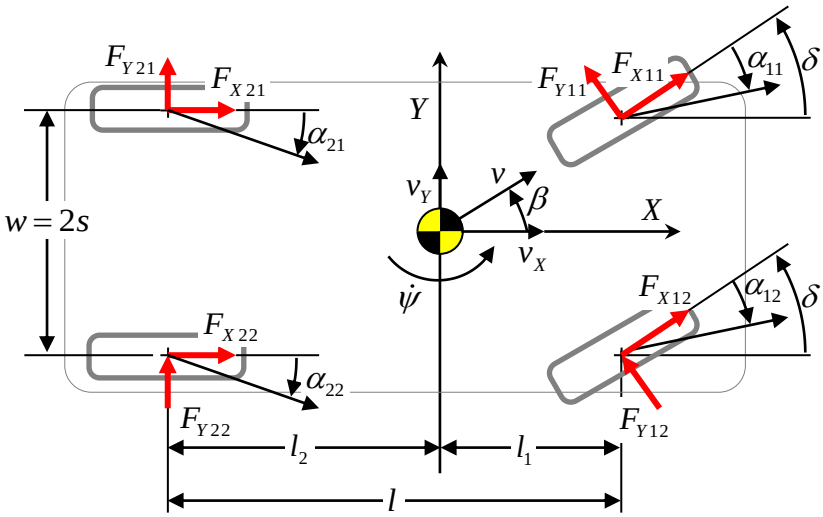

Figure 2.1: Two-track vehicle model

planar vehicle model, the non-linear single track model and the linearized single track model. These models rely in many instances on lumped parameters where a chain of components or subsystem characteristics are combined into a single parameter. The fourth model used in this study is a particle representation of the planar motion. This model is described Paper V.

2.1.1 Two-track Model

The two-track model is used as a basis for the analysis of the case where all the wheel forces are individually controllable. Since the forces from all wheels are modeled separately, the effect of differences in longitudinal forces on the yaw motion is directly considered in the model. This model is used in Papers II, IV and V and is adopted from [23]. The model is illustrated in Figure 2.1 where the individual wheel forces are shown as well as the longitudinal speed, v_X, lateral speed, v_Y, and yaw rate, $\dot{\psi}$, at the center of gravity. Furthermore the figure also shows the steering angle of the front wheels, δ, and slip angles, α_{ij}, where the indices i and j indicate the front/rear axle and the left/right side of the vehicle, respectively. The slip angle is the angle between the velocity vector and the free rolling direction.

Dynamic model From Newton's second law of motion the equations of motion in the longitudinal, lateral and yaw directions are

$$\begin{aligned} ma_X =& (F_{X11} + F_{X12})\cos\delta - (F_{Y11} + F_{Y12})\sin\delta + F_{X21} + F_{X22} \\ ma_Y =& (F_{X11} + F_{X12})\sin\delta + (F_{Y11} + F_{Y12})\cos\delta + F_{Y21} + F_{Y22} \\ mk^2\ddot{\psi} =& -s\cos\delta\,(F_{X11} - F_{X12}) + l_1\sin\delta\,(F_{X11} + F_{X12}) - s(F_{X21} - F_{X22}) \\ &+ s\sin\delta\,(F_{Y11} - F_{Y12}) + l_1\cos\delta\,(F_{Y11} + F_{Y12}) - l_2(F_{Y21} + F_{Y22}) \end{aligned} \tag{2.1}$$

where m is the vehicle mass, k is the radius of gyration and where the longitudinal and lateral accelerations (in the inertial reference frame) are

$$\begin{aligned} a_X &= \dot{v}_X - v_Y\dot{\psi} \\ a_Y &= \dot{v}_Y + v_X\dot{\psi} \end{aligned} \tag{2.2}$$

From Equations (2.1) and (2.2), the following state-space model is derived:

$$\dot{\boldsymbol{x}} = \mathbf{f}_{\text{tt}}(\boldsymbol{x}, \boldsymbol{u}_{\text{tt}}) = \boldsymbol{M}^{-1}\boldsymbol{A}_{\text{tt}}\boldsymbol{T}_{\text{tt}}\boldsymbol{z}_{\text{tt}} - \boldsymbol{a} \tag{2.3}$$

where the state vector and the input vector are

$$\begin{aligned} \boldsymbol{x} &= \begin{bmatrix} v_X & v_Y & \dot{\psi} \end{bmatrix}^\top \\ \boldsymbol{u}_{\text{tt}} &= \begin{bmatrix} F_{X11} & \cdots & F_{X22} & \delta \end{bmatrix}^\top \end{aligned} \tag{2.4}$$

and

$$\begin{aligned} \boldsymbol{M} &= \text{diag}\begin{pmatrix} m & m & mk^2 \end{pmatrix} \\ \boldsymbol{A}_{\text{tt}} &= \begin{bmatrix} 1 & 0 & 1 & 0 & 1 & 0 & 1 & 0 \\ 0 & 1 & 0 & 1 & 0 & 1 & 0 & 1 \\ -s & l_1 & s & l_1 & -s & -l_2 & s & -l_2 \end{bmatrix} \\ \boldsymbol{T}_{\text{tt}} &= \text{diag}\begin{pmatrix} \boldsymbol{T}_1 & \boldsymbol{T}_1 & \boldsymbol{T}_2 & \boldsymbol{T}_2 \end{pmatrix} \\ \boldsymbol{T}_1 &= \begin{bmatrix} \cos\delta & -\sin\delta \\ \sin\delta & \cos\delta \end{bmatrix} \\ \boldsymbol{T}_2 &= \begin{bmatrix} 1 & 0 \\ 0 & 1 \end{bmatrix} \\ \boldsymbol{z} &= \begin{bmatrix} F_{X11} & F_{Y11} & \cdots & F_{X22} & F_{Y22} \end{bmatrix}^\top \\ \boldsymbol{a} &= \begin{bmatrix} -v_Y\dot{\psi} & v_X\dot{\psi} & 0 \end{bmatrix}^\top \end{aligned} \tag{2.5}$$

The lateral forces, F_{Yij}, are a function of the vehicle states, $\boldsymbol{x}$ and the control inputs $\boldsymbol{u}_{\text{tt}}$, as described in the tire modeling section below. First, however, two of the most important factors determining the lateral forces; the vertical forces and the tire slip angle, are described.

Vertical forces The vertical forces forces on all four wheels, F_{Zij}, are given by the static load distribution and the longitudinal and lateral load transfer [28, 48]. This load transfer model, due to longitudinal and lateral acceleration, is

$$F_{Zij} = F^0_{Zij} + (-1)^i \zeta_X m a_X + (-1)^j \zeta_{Yi} m a_Y \tag{2.6}$$

where ζ_{Yi} is the lateral load transfer coefficient of each axle, and the static vertical force and longitudinal load transfer coefficient are

$$\begin{aligned} F^0_{Zij} &= \frac{(l - l_i)mg}{2l} \\ \zeta_X &= \frac{h}{2l} \end{aligned} \tag{2.7}$$

respectively, and where h is the height of the center of mass above the ground and g is the gravitational acceleration.

Slip angles When a wheel is rotated around its vertical axis relative to the free-rolling direction, the tire develops lateral forces [48]. This angle is the slip angle, which is

$$\alpha_{ij} = \delta_i - \arctan \frac{v_{Yij}}{|v_{Xij}|} \tag{2.8}$$

where v_{Xij} and v_{Yij} are the longitudinal and lateral velocities, respectively, of each wheel expressed in the vehicle coordinate system. Note that, in our case, $\delta_1 = \delta$ and $\delta_2 = 0$. The change in sign convention compared to ISO8855:1991 [19], gives that a positive slip angle is associated with a positive lateral force [48]. The use of the absolute velocity in the denominator will avoid numerical problems when v_{Xij} changes sign (vehicle is traveling backwards), and that only the sign of v_{Yij} will determine the sign of the force. Additionally, this definition restricts the maximum possible slip angles to $\pm 90°$, which simplifies the tire model implementation.

By linear transformation of the longitudinal and lateral speed and the yaw rate at the center of gravity to each wheel, the local velocities of each wheel are

$$\begin{bmatrix} v_{Xij} \\ v_{Yij} \end{bmatrix} = \begin{bmatrix} v_X + (-1)^j s\dot{\psi} \\ v_Y - (-1)^i l_i \dot{\psi} \end{bmatrix} \tag{2.9}$$

which, when combined with Equation (2.8) gives that

$$\alpha_{ij} = \delta_i - \arctan \frac{v_Y - (-1)^i l_i \dot{\psi}}{|v_X + (-1)^j s\dot{\psi}|} \tag{2.10}$$

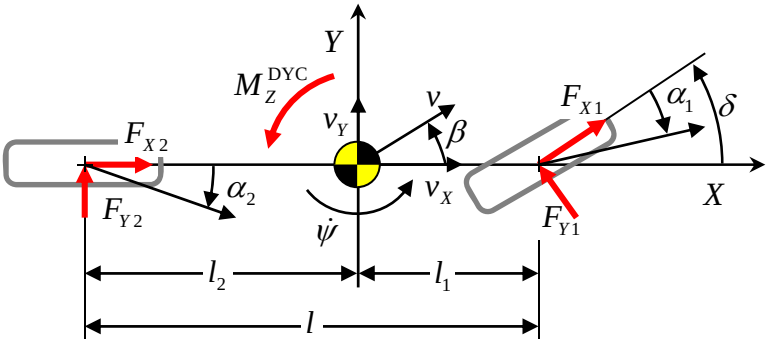

Figure 2.2: Single-track (Bicycle) vehicle model.

Quasi steady-state model In Paper II the quasi steady-state (QSS) approximation [26] is used for cases with a constant total longitudinal force and steering input. This means that when the change in v_X is constant ($\dot{v}_X = c$), and reasonably small, then the lateral and yaw motion can still be considered steady-state, i.e. $\dot{v}_Y = \ddot{\psi} = 0$ [1, 2, 69]. The QSS model therefore implies that

$$\dot{\boldsymbol{x}} = \begin{bmatrix} c & 0 & 0 \end{bmatrix}^\top \tag{2.11}$$

The QSS approximation means that the many handling characteristics that are developed for steady-state cornering, can be applied also when the longitudinal acceleration is not zero, but constant. In Papers I and II the QSS model is used for optimization and study of the longitudinal force distribution of different driveline configurations.

2.1.2 Single-Track (Bicycle) Model

From the two-track model, the single track model, which is illustrated in Figure 2.2, can be deduced. For the single track model, the left/right tires are lumped into an axle equivalent expression. This model is used in Papers I and II and the main advantage of this model is that it is much simpler than the two-track model and thereby simplifies the subsequent analysis of the properties of interest.

Dynamic model The model which is presented here assumes that the differences in longitudinal forces are small, and therefore do not influence the lateral force capability of the tires. The yaw moment that these differences give rise to is denoted M_Z^{DYC}. From the two-track model, the single track model can be derived to be:

$$\dot{\boldsymbol{x}} = \mathrm{f}_{\mathrm{st}}(\boldsymbol{x}, \boldsymbol{u}_{\mathrm{st}}) = \boldsymbol{M}^{-1}\boldsymbol{A}_{\mathrm{st}}\boldsymbol{T}_{\mathrm{st}}\boldsymbol{z}_{\mathrm{st}} - \boldsymbol{a} \tag{2.12}$$

where

$$\begin{aligned}
\boldsymbol{u}_{\text{st}} &= \begin{bmatrix} F_{X1} & F_{X2} & M_Z^{\text{DYC}} & \delta \end{bmatrix}^\top \\
\boldsymbol{A}_{\text{st}} &= \begin{bmatrix} 1 & 0 & 1 & 0 & 0 \\ 0 & 1 & 0 & 1 & 0 \\ 0 & l_1 & 0 & -l_2 & 1 \end{bmatrix} \\
\boldsymbol{T}_{\text{st}} &= \text{diag} \begin{pmatrix} \boldsymbol{T}_1 & \boldsymbol{T}_2 \end{pmatrix} \\
\boldsymbol{z}_{\text{st}} &= \begin{bmatrix} F_{X1} & F_{Y1} & F_{X2} & F_{Y2} & M_Z^{\text{DYC}} \end{bmatrix}^\top
\end{aligned} \tag{2.13}$$

Quasi steady-state model As for the two-track model, the QSS approximation can be used for the single track model in the same way.

Vertical forces The vertical forces from Equation (2.6) are reduced to

$$F_{Zi} = \sum_{j=1}^{2} F_{Zij} = 2(F_{Zij}^0 + (-1)^i \zeta_X m a_X) \tag{2.14}$$

Slip angles The slip angles on each axle, α_i, are the average slip on the left and right wheels which, from Equation (2.10), are:

$$\alpha_i = \delta_i - \arctan \frac{v_Y - (-1)^i l_i \dot{\psi}}{|v_X|} \tag{2.15}$$

2.1.3 Linear Bicycle Model

The vehicle handling characteristics on high friction surfaces, and at low friction utilization, are often considered to reflect the expectations from the driver [66]. The reason for this is that the driver normally operates the vehicle in this region and is therefore assumed to be accustomed to the handling characteristics in that region. As will be seen in the tire modeling section below, the lateral forces are proportional to the slip angle when the friction utilization is low, but will saturate at a constant level for large slip angles.

If the vehicle speed is slowly varying, only the lateral and yaw dynamics of the single-track model (2.3) need to be considered and v_X can be treated as a known parameter. Using a linear tire model where the lateral force is proportional to the cornering stiffness, C_α, and the slip angle, we have that

$$F_{Yi} = C_{\alpha i} \alpha_i \tag{2.16}$$

Using this tire model, the model in Equation (2.3) can be linearized. By linearizing the lateral and yaw degree of freedom in Equation (2.3), combined with Equations (2.15) and (2.16), the following linear state-space model is obtained:

$$\dot{\boldsymbol{x}}_{\text{ref}} = \boldsymbol{A}_{\text{ref}}\boldsymbol{x}_{\text{ref}} + \boldsymbol{B}_{\text{ref}}\boldsymbol{u}_{\text{ref}} \tag{2.17}$$

where the state and input vectors and matrices are

$$\begin{aligned}
\boldsymbol{x}_{\text{ref}} &= \begin{bmatrix} v_{Y,\text{ref}} & \dot{\psi}_{\text{ref}} \end{bmatrix}^\top \\
\boldsymbol{u}_{\text{ref}} &= \begin{bmatrix} \delta & M_Z^{\text{DYC}} \end{bmatrix}^\top \\
\boldsymbol{A}_{\text{ref}} &= -\frac{1}{m|v_X|}\begin{bmatrix} C_{\alpha 1}+C_{\alpha 2} & l_1C_{\alpha 1}-l_2C_{\alpha 2}+v_X^2 \\ (l_1C_{\alpha 1}-l_2C_{\alpha 2})/k^2 & (l_1^2C_{\alpha 1}+l_2^2C_{\alpha 2})/k^2 \end{bmatrix} \\
\boldsymbol{B}_{\text{ref}} &= \frac{1}{m}\begin{bmatrix} C_{\alpha 1} & 0 \\ l_1C_{\alpha 1}/k^2 & 1/k^2 \end{bmatrix}
\end{aligned} \tag{2.18}$$

respectively. This model can be used as reference model for feedback control, of which an example will be given in the next chapter. The reference yaw rate is in Paper IV limited to that which is attainable on a dry surface. The reference yaw rate is therefore limited to be no more than

$$|\dot{\psi}_{\text{ref}}| \leq \frac{\bar{a}_Y - |\dot{v}_Y|}{v_X} \tag{2.19}$$

where $\bar{a}_Y$ is some pre-determined maximum steady-state lateral acceleration. Note that, by limiting the yaw rate, the model is again non-linear.

2.2 Tire Models

Simple tire models are used throughout this study. This is in agreement with the primary objectives of this study to focus on studying the fundamental – qualitative – behavior of the vehicle dynamics properties. Numerous tire models are available in the literature ranging from linear tire models with a single parameter (cornering stiffness) to over one-hundred parameters for the Magic Formula and SWIFT model [7, 48, 59]. The Magic Formula tire model is perhaps the most well-known and due to the number of parameters, it can fit tire measurements very well.

As pointed out in [48], however, the better the fit to tire data, the less insight in the tire physics is generally provided due to the increased complexity of the model. The requirements we have on the model (apart from it being simple) are that the model should provide:

- Good qualitative description of lateral force for a large range of slip angles.

- Combined slip model using either longitudinal slip or longitudinal force as inputs to describe the influence on the lateral force generation.

Tire models commonly use slip quantities as input and forces and moments as output. Slip is defined as a deformation of the rubber of the tire in a particular direction due to an angle or speed difference of the wheel relative to a free-rolling wheel. The slip quantities and associated forces which are of interest in this study are the longitudinal slip, κ, lateral slip angle α and the longitudinal and lateral forces. In particular the influence of the longitudinal and lateral slip (or associated force) on the steady-state lateral force generation is in focus.

Two different combined slip models and two different force versus slip models are used so both will be given separately. The combined slip and force versus slip models are combined independently. This combination results in

$$F_Y = \chi F(\sigma), \tag{2.20}$$

where $F(\sigma)$ and χ are the force magnitude and combined slip models, respectively.

Since the most commonly used method in the literature is to use longitudinal slip for the combined slip model and that this study primarily uses longitudinal force as input [48], a comparison between the two approaches is made.

Force Magnitude Model The force magnitude is here assumed to be a function of either the combined slip or only the lateral slip, depending on the combined slip model. The two most significant parameters of the tire model are the cornering stiffness (slope of force/slip through the origin) and the peak force. These factors are determined by the tire characteristics, tire/road friction and the vertical load on the tire. Depending on the road surface, two simple force models have been used:

- Two parameter isotropic saturation model for low-friction surfaces
- Three parameter isotropic model with distinct peak for high friction surfaces

The simple saturation model works well for low friction surfaces which typically do not exhibit a clear peak in the lateral force, whereas such a peak is typical on high friction surfaces such as dry asphalt. The three parameter model is a simplified version of the Magic Formula tire model. These models are

$$F_1 = D\sin(C\arctan(B\sigma)) \tag{2.21}$$
$$F_2 = D\tanh(CB\sigma) \tag{2.22}$$

For the high-friction model (F_1), the vehicle slip σ^* for which the maximum force is obtained ($F_1 = D$) is

$$\sigma^* = \frac{1}{B} \tan \frac{\pi}{2C} \tag{2.23}$$

The other model instead saturates at to a constant force for large slip values.

The tire parameters B, C and D are determined for a particular vertical load and camber angle. These parameters can also be adjusted to include effects of suspension and steering compliance [48]. These considerations are why these parameters, in general, are different for the front and rear suspension although the same tires are used.

Combined Slip Model The combined slip models are adopted from [48] and are

$$\chi_1 = \sqrt{1 - \left(\frac{F_X}{\mu F_Z}\right)^2}, \quad \forall |F_X| \leq \mu F_Z \cos\alpha \tag{2.24}$$

$$\chi_2 = \sigma_Y / \sigma \tag{2.25}$$

The first model uses the longitudinal force, F_X, as input and the other model uses the longitudinal slip, κ as input. The limitation on the longitudinal force in Equation (2.24) is such that for a locked or spinning wheel, the wheel is viewed as a sliding block, i.e. $F_X = \mu F_Z \cos\alpha$ and $F_Y = \mu F_Z \sin\alpha$.

For the second model, χ_2,

$$\sigma = \sqrt{\sigma_X^2 + \sigma_Y^2} \tag{2.26}$$

and

$$\begin{bmatrix} \sigma_X \\ \sigma_Y \end{bmatrix} = \frac{1}{1+\kappa} \begin{bmatrix} \kappa \\ \tan\alpha \end{bmatrix} \tag{2.27}$$

Comparing different combinations of the force magnitude and combined slip models The two combined slip and force magnitude models are compared in Figures 2.3.a and 2.3.b, respectively. Both sub-figures show the normalized lateral force as function of slip angle α. The two combined slip models show good correlation and so do the two force magnitude models. Usually the tire operation regions are divided into a linear operating region which in Figure 2.3 is for $|\alpha| < 5°$; a nonlinear region for $5° < |\alpha| < 10°$; and a saturation region for $|\alpha| > 10°$. The main difference between the two combined slip models (a) is in the linear region for large longitudinal forces, the cornering stiffness (slope through the origin) is slightly overestimated for the model that uses F_X as the input.

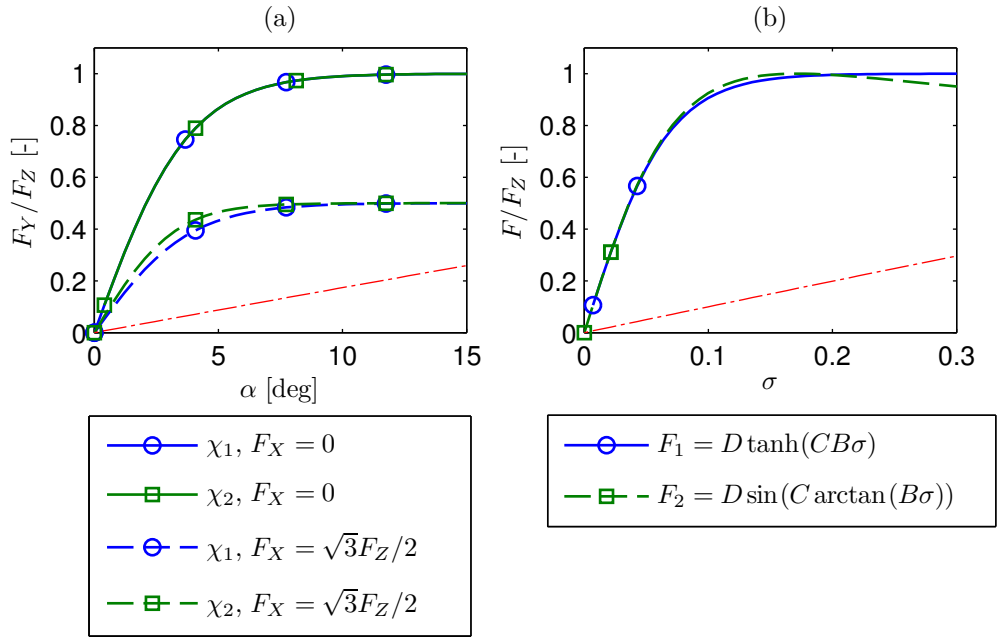

Figure 2.3: Comparison of two different combined slip models (a) and to two different force magnitude models (b). The dash-dotted line is the force for a locked or spinning wheel when $F_Y = \mu F_Z \sin\alpha$

In Figure 2.4, F_Y and F_X for different levels of constant κ and α are shown which further illustrates the effect of combined slip.

The two tire characteristics which are mostly used in this work are the lateral grip, $F_Y^{\lim}$ and the (effective) cornering stiffness, C_α. These are important since the lateral grip on either axle will determine the lateral grip of the entire vehicle and the cornering stiffness of the tires determine the understeer of the vehicle. The lateral grip for each tire is

$$F_Y^{\lim} = \chi D = \chi \mu F_Z \tag{2.28}$$

where μ and F_Z are the friction coefficient and vertical force, respectively. The lateral grip of an axle is simply the sum of the lateral grip of the tires on that axle. The cornering stiffness is

$$C_\alpha = \left.\frac{\partial F_Y}{\partial \alpha}\right|_{\alpha=0} = \chi BCD \tag{2.29}$$

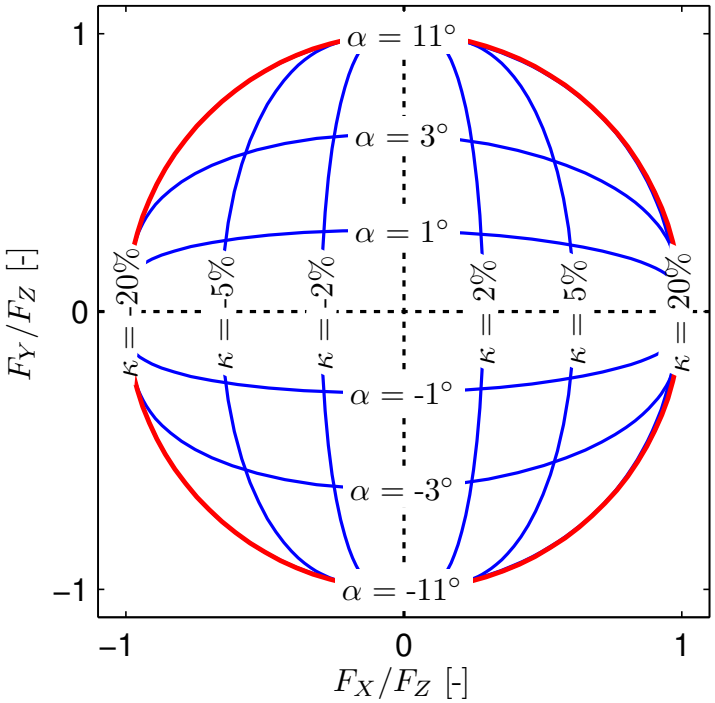

Figure 2.4: F_Y and F_X for different levels of constant κ and α

2.3 Comparison of Vehicle Models

The different vehicle models presented in Section 2.1 are compared for two different open-loop maneuvers. The vehicle and tire data is from Paper V and the steering wheel to steer angle ratio is 16:1. The tire models used in this comparison are χ_1 and F_1. The results presented in Figure 2.5 show the yaw rate, $\dot{\psi}$, and side-slip, β, which are the response to a 0.5Hz half-period sine steering wheel impulse [18, 20] input with two different amplitudes. It can be seen from Figure 2.5.a and 2.5.b that for the low amplitude steering input, the response from all three models are nearly identical. The reason for this correlation is that the tires, for this small steering input, are excited in the linear operating region only. For a large steering input as shown in Figure 2.5.c and 2.5.d, the differences in the models are more significant, as expected.

Similar results can be seen when making a comparison of the vehicle response to a ramp on the steering input as shown in Figure 2.6. For small steering inputs, the three models give the same response, but for more steering the yaw rate and side-slip of the different models diverge as the tires saturate.

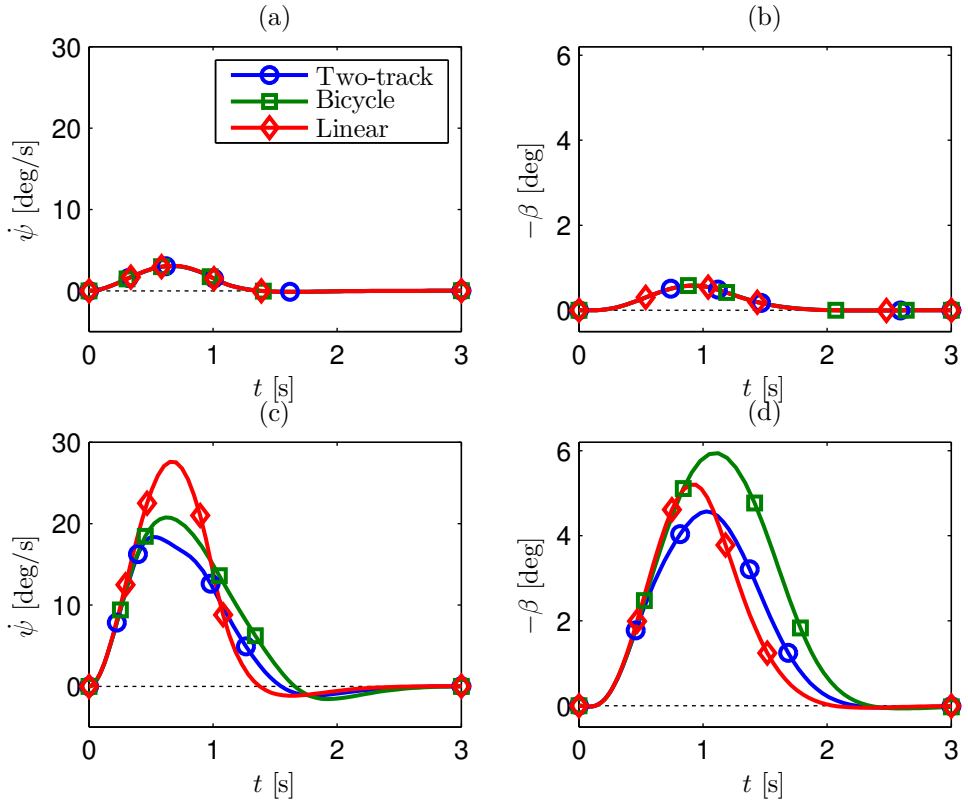

Figure 2.5: Response to a 0.5 Hz half sine steering input at 144km/h. The steering wheel angle amplitude is $5°$ for (a) and (b) and $45°$ for (c) and (d).

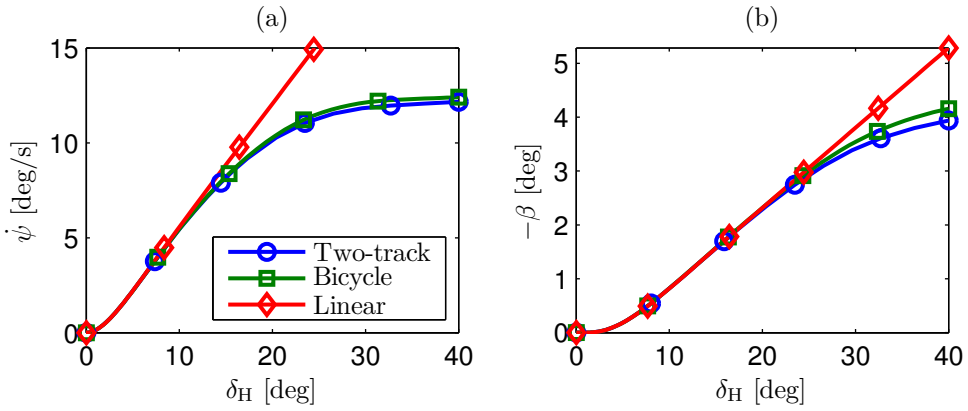

Figure 2.6: Response to a ramp steer (10°/s) maneuver.

2.4 Driveline Systems

Although no driveline dynamics is considered in this study, the general layout of a general mechanical driveline is taken into account. This is done to make it easier to relate the implications of the obtained results to actual driveline actuators such as clutches, differentials and other driveline components.

The powertrain starts with a power source – for example an internal combustion engine (ICE) or electric motor (EM) – that drives more than one output in which case drive force is divided through a power split device [27]. In this section, some different power split devices and how the drive force is distributed by these devices are discussed.

Apart from the role of the power-split device in the drive force distribution, it may be relevant also to understand the nature of the power source. One simple mathematical model that can be used to constrain the maximum drive force for both an ICE as well as an EM is

$$F_X^{\text{IN}} \leq \min(F_X^{\text{lim}}(n), P^{\text{lim}}/v_X), \tag{2.30}$$

where F_X^{IN} is the output from the power source, $F_X^{\max}(n)$ the maximum force for the selected gear n and P^{lim} is the maximum mechanical power. An example force-speed map for a particular combination of ICE and transmission combination from Paper III is shown in Figure 2.7. There it can be seen how the maximum force for lower speeds is limited by the engine's torque limit and for higher speeds is limited by the maximum power of the engine.

The most commonly used power split device is the (open) differential which has one input and two outputs. Without any friction, a differential divides the drive torque to each output with a fixed ratio (often 50:50) regardless of the speed difference between the outputs. If the engine drives all four wheels, three power split devices are necessary. Since the free-rolling wheel speeds on all four wheels typically are different while cornering, restricting or superimposing a speed difference will generate a longitudinal force difference between the outputs which will affect the cornering of the vehicle. The benefit of the differential is that the speed difference on the outputs can be arbitrary while the torque ratio between the two outputs is always constant (assuming no friction). This means that the cornering behavior is not influenced as a result of interconnecting the wheels through the driveline.

Although in most instances equal drive force distribution on the output shafts is desirable, there are exceptions to this. One such instance is if the tire/road friction at the different axles or wheels are very different. In this case, the total longitudinal force is limited by the wheel with the least friction. By introducing friction in the differential, however, the ratio between the drive forces on the output shafts can be different than the mechanical ratio and thereby provide better

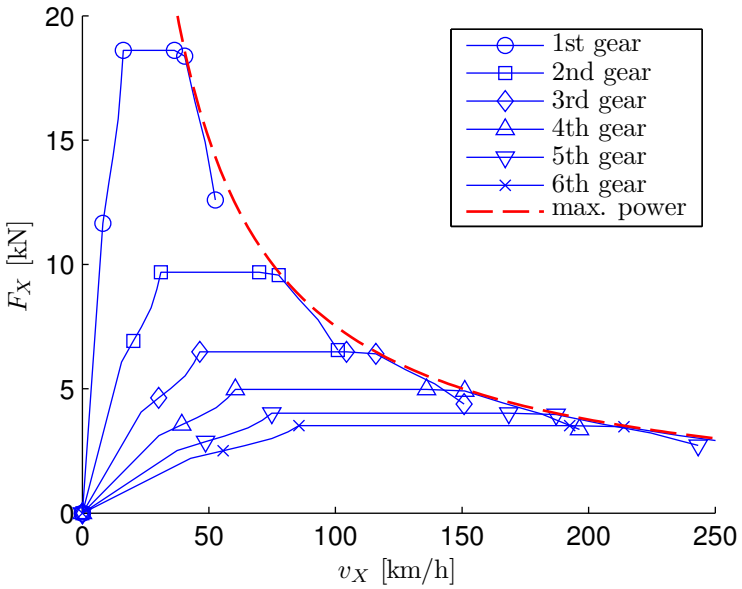

Figure 2.7: Maximum engine force per gear as function of vehicle speed. This particular engine has a torque limit of 400Nm and a power limit of 280hp.

overall traction. This ratio is called the torque bias ratio which is defined as

$$\eta = \frac{M_{\text{high}}}{M_{\text{low}}} = \frac{\max(M_1, M_2)}{\min(M_1, M_2)} \tag{2.31}$$

where, M_1 and M_2 are the torque on the first and second output shaft, respectively. In order to illustrate the effect of friction in the differential on the traction performance the relative traction (relative to the traction if the resistance on both outputs were equal) versus the ratio between the high and low friction outputs for three different configurations is shown in Figure 2.8. There it can be seen that the relative traction for an open differential is zero if the friction on the low-friction side is zero. If instead the differential is locked, the traction capacity on the high-friction output can be fully utilized.

Differentials with friction are called limited slip differentials (LSD), since the speed difference is limited by added resistance between the outputs. The friction can be proportional to the speed [49] or torque difference [9] between the output shafts or be actively controlled. An example of an electronically controlled LSD (eLSD) is presented in Paper III where the friction can be actively varied by controlling the hydraulic pressure in a clutch. A principle sketch of an eLSD is shown in Figure 2.9.b, where actuation of the clutch restricts the speed difference between the input and one of the outputs. Since the outputs are connected through the differential, this will also restrict the speed difference between the two outputs.

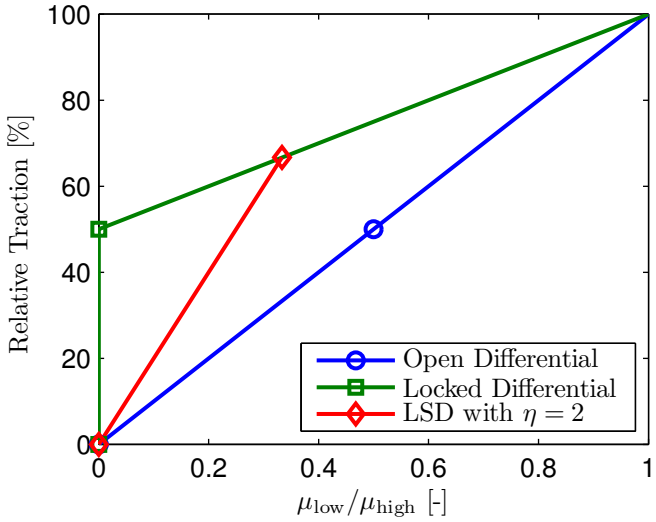

Figure 2.8: Relative traction of an axle depending on the friction ratio between the low and high friction of the two wheels. The same principle can be applied to the relative traction between the front and rear axle.

Apart from the (LSD) which *restricts* the speed difference between the outputs, there are so-called torque vectoring differentials (TVD) which can *impose* a speed difference. These differentials are advanced mechanical devices which are typically composed of an open differential and two gear sets which – when engaged – causes the outputs of the differential to rotate with a fixed speed difference in either direction (one direction per gear-set). The concept shown Figure 2.9.a is a TVD having a fixed left/right speed difference across two controllable clutches, which connect the left and right drive shafts when engaged. This particular TVD is described in more detail in references [16, 54, 56]. Other mechanical implementations of the same principle, but using a speed increasing/decreasing mechanism on each side of the differential using planetary gears, is given in [34] or an elegant solution using epicyclic gears in [60].

In addition to the open, limited slip and torque vectoring differentials, a clutch placed between one input and one output, is also possible to be used for torque transfer [41, 50, 64]. In Paper I four different front/rear drive force distribution configurations are presented. There the effect modulating between an open and locked clutch depending on where it is placed in the driveline is discussed. Typically the clutch is placed between the front and rear wheels where the power source is directly connected to either front or rear axle. In Paper III, the clutch is used to modulate the drive force transfer to the rear wheels.

As mentioned in the introduction, many consider individual drive on each

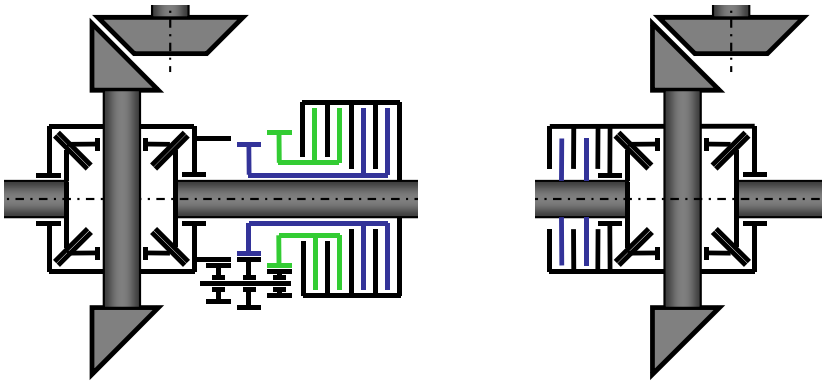

a.) Torque vectoring differential (TVD) b.) Limited slip differential (eLSD)

Figure 2.9: Examples of two different rear differential units.

wheel as the ultimate all-wheel drive technology. Already with the presence of two power sources driving different axles, a wide range of difference in the front/rear drive force distribution becomes possible. Further developments, such as torque vectoring systems using electric motors, may eventually lead to full freedom in the distribution of the longitudinal forces on each wheel.

Chapter 3

Longitudinal Forces and Yaw Stability

The objective of this chapter is to provide the reader with an overview of the effects of longitudinal force distribution on the yaw stability of the vehicle. Particular attention is given to differences in the left/right drive force distribution. It will be shown that the yaw moment that arises from these differences has a significant influence on the yaw stability of the vehicle. The specific motivation of this chapter is that the focus of all papers except Paper IV is mainly on road holding, and that some additional discussion on yaw stability is therefore warranted, given its importance to vehicle handling. This means that the vehicle response to inputs from the driver (steering, throttle, brakes) and/or external disturbances should not cause excessive yaw motion and/or leading to large side-slip angles.

The yaw stability aspects are divided into analyzing the convergence properties of solutions around a steady-state condition and the dynamic stability, which here is defined as the rate of convergence after large deviations from steady-state conditions. Firstly the influence of a constant turn-in yaw moment on the yaw stability is studied. Secondly the effects of using individual braking to stabilize excessive yaw motion or adding additional yaw damping to the system by locking a differential are analyzed.

Stability analysis is a large subject, and this chapter only intends to provide an overview of the yaw stability properties of the vehicle dynamics system. The interested reader is referred to [26] for stability of general non-linear systems and an excellent reference for stability for a wide range of vehicle systems (including aircraft) is presented in [24].

In this chapter, first a motivational example will be presented to highlight that yaw stability must be considered when applying a turn-in yaw moment. Next, the influence of the understeer on the yaw stability of the linear bicycle model is discussed. Subsequently the handling diagram is presented, for which the understeer can be determined also for the non-linear operating region of the vehicle. Using

the handling diagram, the case where a turn-in yaw moment can cause the vehicle to change from understeer to oversteer, and thus may become unstable, is studied in detail. This case is further analyzed using phase-plane diagrams, where the dynamics of an autonomous non-linear system can be visualized. After discussing solutions for a system with statically stable solutions, but which still may be considered unstable for some instances, a brief introduction to yaw stability control and yaw damping strategies, will conclude the chapter.

3.1 Yaw Stability and Closed-loop Yaw Control in the Presence of Understeer

The ability to control the curvature of the path is essential for safe operation of the vehicle. This road holding ability is in Papers I and II studied from the perspective of the road holding capability – lateral grip – of the vehicle. In Paper V the case is studied where the entry speed is too high for the vehicle to track a particular curve, given the available lateral grip. Such a situation is commonly referred to as terminal understeer [37]. To mitigate the understeer, one commonly proposed strategy is to increase the yaw rate for the curvature to increase [42]. If, however, the yaw rate is increased beyond the lateral grip, instead the vehicle side-slip will increase, thereby compromising the yaw stability.

In order to illustrate such a case, consider the (somewhat idealized) example shown in Figure 3.1. Here three vehicles are all turning at the grip limit of the vehicle and surface and with the same yaw rate. This could be the case if the vehicles are following a common yaw-rate reference using a yaw control system [66].

It can be seen in Figure 3.1 that following the same yaw rate for three different surfaces may lead to very different outcomes for path following and yaw stability, with excessive side-slip occurring on low friction surfaces. This excessive side-slip will lead to loss of yaw stability, which may be uncontrollable for the driver. A common way for the active yaw control system to avoid a too large yaw rate is to limit the reference/target yaw rate by taking the (estimated) surface friction into account [14, 66]. Such a strategy will prevent yaw instability, but does nothing to improve path curvature; and when a driver makes a large steering input, it is likely that the intention really is to increase the path curvature. The conclusion of this is that the focus of the study should firstly be at optimizing the force magnitude and direction and only secondly on the yaw rate following. This is also one motivation for the particle model approach used to solve such problems in Paper V.

From this example it is obvious that, apart from the ability to change the path curvature, the yaw stability is also essential for safe operation of the vehicle.

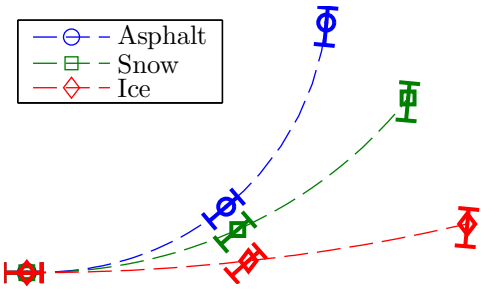

Figure 3.1: Example of vehicle motion on three different surfaces with the same speed and yaw rate.

3.2 Yaw Stability for the Linear Bicycle Model

Stability for the linear bicycle model can be determined by eigenvalue analysis of the state matrix ($\boldsymbol{A}_{\text{ref}}$ in Equation (2.17)). For the model to be stable for a particular speed, the real part of the eigenvalues must be negative [26]. Here, the study is limited to analyzing the stability of the yaw motion as response to changes in the steering input. To do so, the influence of the longitudinal speed and vehicle parameters on steady-state gain of the steering to yaw rate is studied.

From the linear bicycle model (Equation (2.17)) the steady-state yaw rate gain from the steering input is obtained:

$$\frac{\dot{\psi}}{\delta} = \frac{v_X}{l + K_u v_X^2} \tag{3.1}$$

where

$$K_u = -\frac{m}{l}\frac{l_1 C_{\alpha 1} - l_2 C_{\alpha 2}}{C_{\alpha 1} C_{\alpha 2}} \tag{3.2}$$

is identified as the understeer coefficient of the linear bicycle model. For the yaw stability of a road vehicle, the understeer is an important steady-state characteristic. It can be seen from Equation (3.1) that the steady-state gain tends to infinity when the denominator tends to zero; which means that the yaw motion is unstable. For this to occur the understeer must be negative ($K_u < 0$) and $v_X = \sqrt{-l/K_u}$, which is the *critical* speed. For a more detailed discussion on the relationship between the understeer and stability the interested reader is referred to [3, 24, 48].

3.3 Handling diagram

The results which are obtained from the handling diagram [24, 47, 48] are the similar as the experimental results from a vehicle test such as the ISO-4138 [21]

steady-state cornering test. From this test the understeer and the lateral grip, for both the linear and non-linear operating region, can be determined and the handling diagram is a useful tool to visualize these results.

In order to give some background useful to the understanding of the handling diagram, some kinematic relationships of a turning vehicle are given in Figure 3.2. The solid circle to the top left is the vehicle's instantaneous center of rotation. The front and rear slip angles in the figure are α_1 and α_2, respectively. If the test is performed with a constant cornering radius, R, and the tangential speed is increased, then also the slip angles increase. Note that in the figure, the scale of the vehicle is exaggerated relative to the cornering radius. In all instances relevant to this study, $l \ll R$, therefore small angles approximations are used. From Figure 3.2 it can be seen that

$$\delta - l/R = \alpha_1 - \alpha_2 \tag{3.3}$$

Note in particular that if the speed of the vehicle is low the slip angles are zero then $\delta = l/R$. This angle is referred to as the Ackermann angle [48].

In Figure 3.3 the normalized lateral force versus tire slip angle is shown in Figure 3.3.a and the handling diagram in Figure 3.3.b. In the handling diagram, the lateral acceleration is treated as the independent parameter, but is shown on the ordinate axis to aid the comparison with the normalized lateral forces of each axle. In the handling diagram the difference between the front and rear slip angles are then shown relative to the lateral acceleration.

The understeer of the vehicle is defined as [21]:

$$K_u = -\frac{\partial(\delta - l/R)}{\partial a_Y} = -\frac{\partial(\alpha_1 - \alpha_2)}{\partial a_Y} \tag{3.4}$$

which is the slope of the handling curve in Figure 3.3.b. It is straightforward to verify that the expression in Equation (3.2) can also be obtained by using this definition, the linear tire model (2.16), the yaw balance, and the turning geometry in Figure 3.2. The linear slope of the handling curve is in Figure 3.3.b accentuated with the line with diamond markers.

The lateral grip can be seen in the diagram as the peak lateral acceleration indicated with an asterisk in Figure 3.3.b. Comparing Figure 3.3.a and 3.3.b one can see that the lateral grip is limited by the front axle in this case. Also, since normalized cornering stiffness (slope in 3.3.a) is less for the front axle than for the rear, the understeer is always positive. More examples of handling diagrams for different tire characteristics are given in [24] and [48].

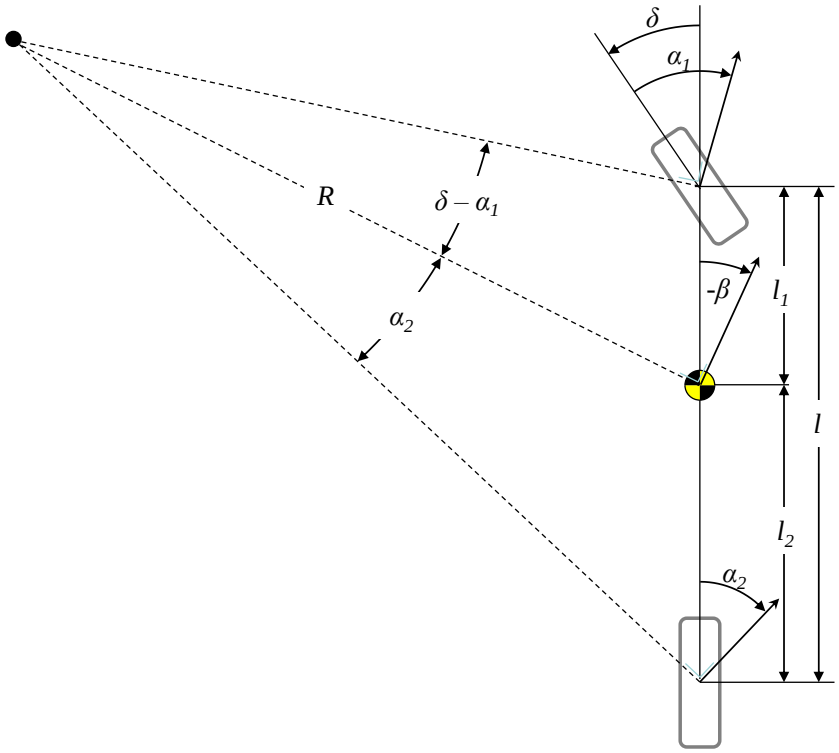

Figure 3.2: Relationship between wheelbase, slip angles, steering angle and the cornering radius. The solid circle to the top left is the vehicle's instantaneous center of rotation.

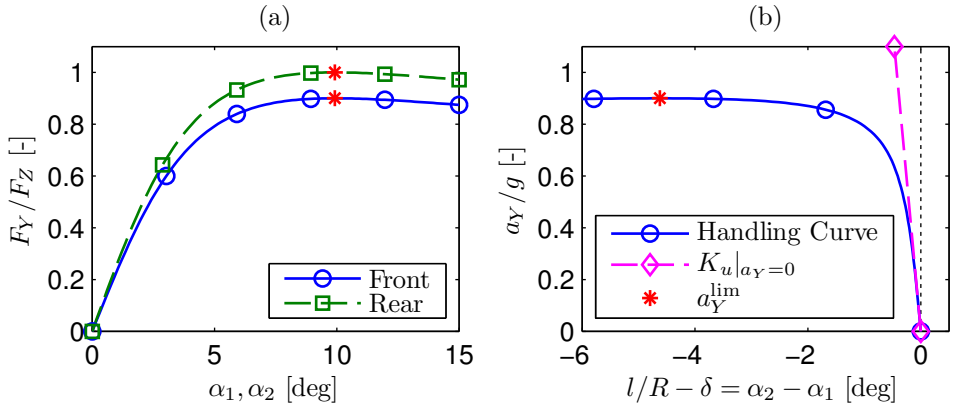

Figure 3.3: Normalized axle lateral force/slip characteristics (a) and the handling diagram showing the understeer of the vehicle (b) relative to the slip angle difference.

3.4 Stability and the Handling Diagram

This stability discussion deals with the stability properties for small perturbations around a particular steady-state condition. Here we will study the influence of a turn-in yaw moment on the yaw stability. One example will be given where this yaw moment can change the behavior of the vehicle, from being statically stable for any lateral acceleration to being stable for small but unstable for large lateral accelerations.

If the yaw moment is such that $K_u < 0$ for some combination of v_X and δ, the vehicle may become unstable for that yaw moment [24, 48].

In Figure 3.4 two different cases are studied. One is without any additional yaw moment (circle markers) and the second (square markers) with a yaw moment such that the lateral grip is maximized. This yaw moment provides that both front and rear axles reach the lateral grip simultaneously, and can be identified in the MMM-diagram in Paper IV as the vertical distance between the right or left vertex and the abscissa of the diagram.

Given that the yaw moment and the speed are fixed, the lateral acceleration at which the vehicle will become unstable is the point where the slope of the handling curve is parallel to the straight line that relates the lateral acceleration to the Ackermann steering (l/R) for a given speed [48] (indicated with triangles for 90km/h in Figure 3.4). This point is marked with an asterisk in Figure 3.4. It can also be seen from the right handling curve (which changes from understeer to oversteer) that, for the same steering input, two different lateral accelerations can be reached. The lower lateral acceleration is a stable steady-state condition and the point above the asterisk is unstable.

It may further be noted that the unstable steady-state condition can also be reached with a (large) steering input in the opposite direction (right of the Ackermann curve). This means that, while turning left, the steering is in the right direction. This condition is referred to as drifting, studied in [11, 45, 67, 68], for instance.

3.5 Dynamic Stability

Non-linear systems may have multiple steady-state solutions with different qualitative behavior [26], as could be seen in the previous section. One useful method to visualize qualitative behavior for large deviations from the steady-state solution is the phase portrait. Since the method is limited to systems with two state variables, the phase portrait is generated for the side-slip β and the yaw velocity $\dot{\psi}$ using a fixed longitudinal speed and steering input.

In Figure 3.5 an example of a phase portrait using the bicycle model (2.12) is

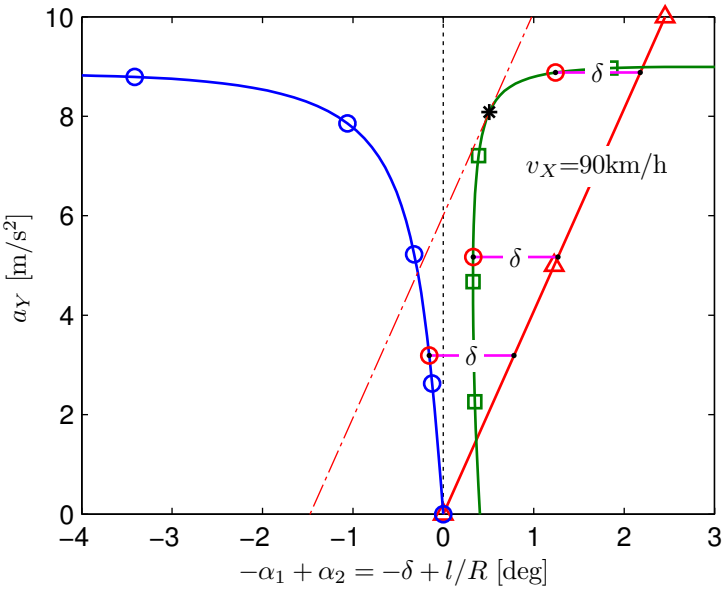

Figure 3.4: Handling diagram for a fixed 15° steering wheel input at a velocity of 90km/h. The straight inclined lines marked with a given speed relate the lateral acceleration to the path curvature for that speed.

shown, thereby using the same speed and steering input as for the right handling curve in Figure 3.4. Since a sufficiently large turn-in yaw moment is applied to the vehicle, an additional equilibrium appears. This equilibrium is characterized as a saddle node [26] since a linearization of the bicycle model around this equilibrium results in one stable (negative real part) and one unstable (positive real part) eigenvalue. The two equilibrium points in Figure 3.5 are the same as the two points for the right handling curve in Figure 3.4 that equate to 15° steering wheel angle input (marked with horizontal lines). The lateral acceleration at each equilibrium is $a_Y = v_X\dot{\psi}$.

The bold curve through the saddle node is the separatrix which separates the stable and unstable manifolds of the phase portrait. By linearizing the system around the saddle node, the eigenvector associated with the stable eigenvalue gives an (conservative) approximation of the separatrix. This approximation is in Figure 3.5 shown by the dashed diagonal line through the saddle node. The normalized distance between any point in the state-space to the separatrix could be viewed as a stability margin.

Even though there is only a stable focus in the phase-plane (no saddle nodes), there may still exist solutions that are considered unstable. This is for the case when $M_Z^{\mathrm{DYC}} = 0$, corresponding to the left handling curve in Figure 3.4. One particularly severe maneuver for yaw stability is the sine-with-dwell maneuver

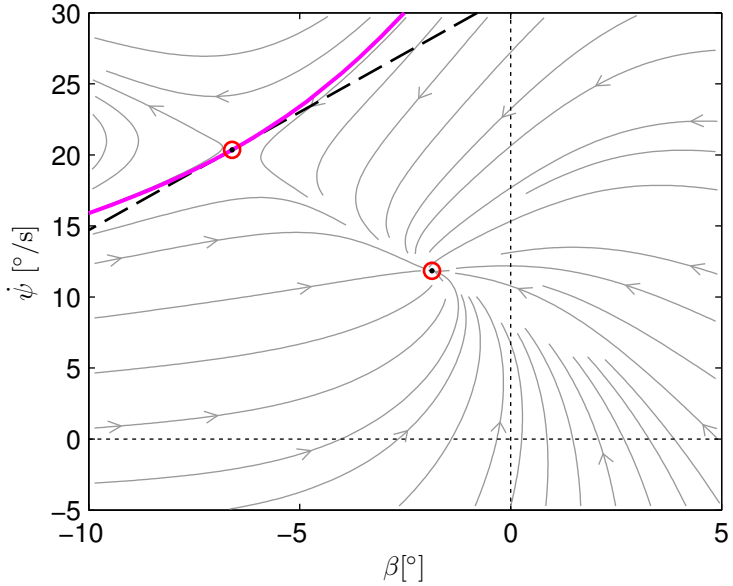

Figure 3.5: Phase portrait for a fixed 15° steering wheel input at a velocity of 90km/h. Shown are also the separatrix (bold solid) and the equilibrium points (circles).

[43], which is developed to evaluate the yaw stabilization ability of an ESC system. During this maneuver, a rapid steering cycling of the steering input causes the lateral forces to act out of phase during a short period, generating a large yaw motion. Unless the yaw motion is stabilized, sufficiently large amplitudes of the steering input causes unacceptably large (unstable) changes in the heading direction of the vehicle.

In Paper IV the stability criteria of the sine-with-dwell maneuver are related to Lyapunov stability [12, 26]. The stability criteria for this maneuver are such that the yaw rate must converge to zero "sufficiently fast" after the steering input is brought back to zero [43]. In Figure 3.6, a phase portrait for $\delta = 0$ and $v_X = 25$ m/s is shown together a contour of the gradient for a simple quadratic Lyapunov candidate function. The contour presented in the phase-plane is where gradient is zero:

$$\dot{V} = \dot{\psi}\ddot{\psi} + \eta^2 \beta\dot{\beta} = 0, \tag{3.5}$$

where η is tuned such that $\dot{V} \approx 0$ when the stability criteria in [43] are just met. This means that we can relate a well-known stability criterion, namely the Lyapunov stability to the stability criteria in [43] and analyze the results in a phase portrait.

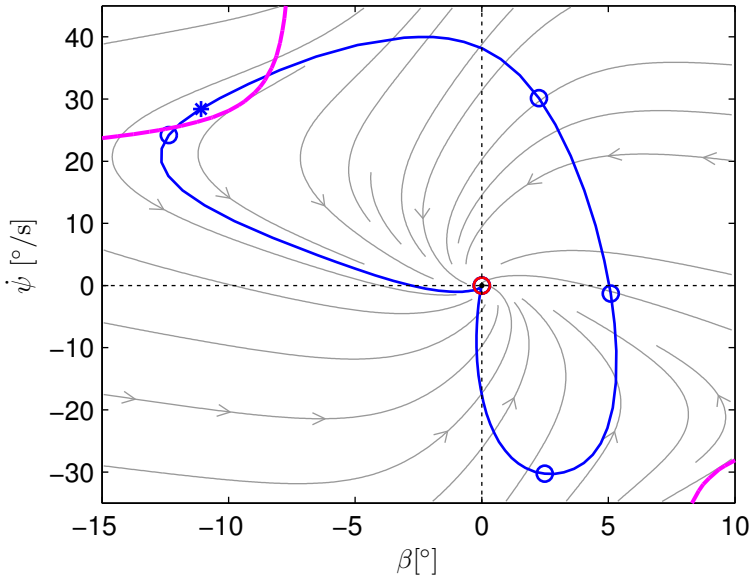

Figure 3.6: Phase portrait and the state history of a Sine-with-Dwell maneuver. In the upper left and lower right corners, the contour of the Lyapunov gradient surface where $\dot{V} = 0$ is shown. The asterisk marks where the steering input is completed.

3.6 Yaw Stability Control

In order to avoid loss of yaw stability, yaw stability control is applied using longitudinal forces to generate a counteracting yaw moment. The yaw stability control is in Paper IV based on a simple proportional controller, braking the outer front wheel when a certain limit of deviation between the actual yaw rate and the reference yaw rate is detected. The control diagram for this system is shown in Figure 3.7. Although the system inevitably will slow down the vehicle, the yaw stability control system is an excellent example of how to use longitudinal forces to accomplish a large safety benefit.

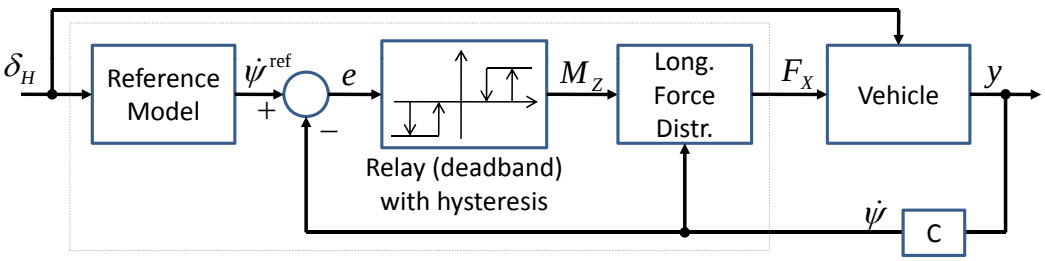

Figure 3.7: Yaw stability control diagram.

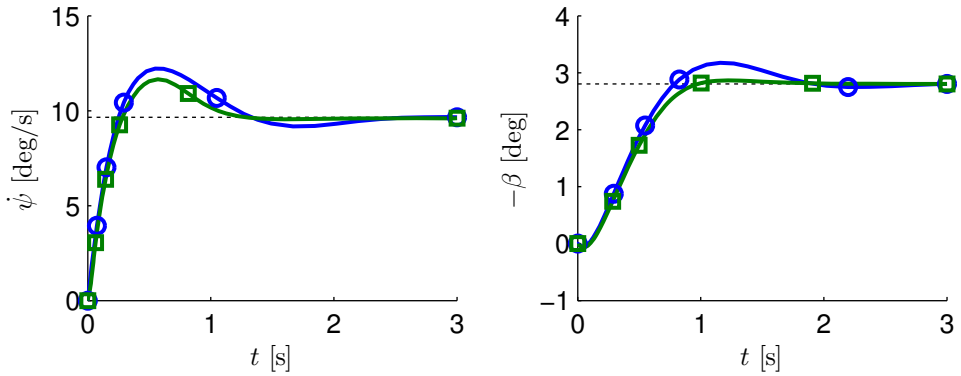

Figure 3.8: Passive vehicle (circle markers) and yaw damping (square markers).

3.7 Yaw Damping

Rapid changes in the steering input during high-speed driving or a sudden throttle off in a turn can be additional areas where yaw stability could become compromised. In contrast to the yaw stability control described earlier, no changes in the steady-state characteristics are aimed for. Also, in general no reduction in speed is accomplished meaning that the intervention can be made more often than an ESC intervention.

The throttle off in a turn, studied in Paper III, causes an instant reduction in turning radius due to the longitudinal load transfer as discussed in Paper I. There it is shown that the eLSD can provide significant improvements in the yaw damping.

Here, a simple derivative control on the deviation between the actual and reference yaw rate is combined with gain scheduling. The results for a step-steer are shown in Figure 3.8. There it can be seen that significant improvements in the damping of the yaw motion can be achieved. It can further be seen in the figure that a properly designed yaw damping strategy does not effect the rise-time or the steady-state gain.

Chapter 4

Summary of Appended Papers

This chapter chapter summarizes the main points and context of the appended papers.

4.1 Paper I – Front/Rear Drive Force Distribution

The objective of this paper is to describe the combined longitudinal and lateral road holding capability with the simple single-track model. To facilitate a better correlation of the single-track model to more complex models, closed-form expressions that better describe critical axle performance parameters than currently used approximations, are necessary. The expressions for the lateral grip limits and the vehicle understeer are therefore developed to account for general cases of front/rear drive force distributions.

The dynamic square method, presented in **(author?)** [25], is used to show the effect of an arbitrary front/rear drive force distribution on the lateral grip. Using this diagram the optimal front/rear drive force distribution can be graphically identified. Another objective of this paper is to extend the dynamic square method so that both the grip limit and the understeer can be analyzed under conditions with constant longitudinal acceleration.

The developed single-track model and extensions to the dynamic square method are applied to four particular driveline configurations, thereby demonstrating the application of these methods for analysis of modern driveline systems.

4.2 Paper II – Optimal Force Distribution

As in Paper I, the influence of drive force distribution in AWD vehicles is in this paper studied from the aspects of lateral grip and vehicle understeer when

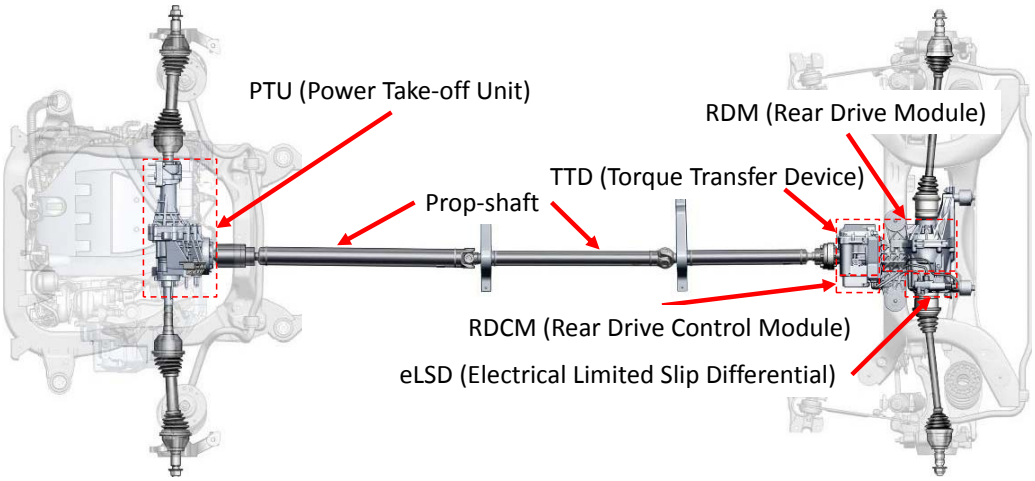

Figure 4.1: Saab XWD System

accelerating in a turn. In this paper, however, the scope is expanded to also include the effects of left/right drive force distribution.

In this paper a new method of optimizing the longitudinal force distribution for combined traction/braking and cornering is studied. In order to provide a general, simple and flexible problem formulation, the optimization is addressed as a quadratically constrained linear programming (QCLP) problem. This method gives fast numerical solutions and makes it also possible to conveniently include a wide range of different driveline configurations to the problem formulation.

Optimizing the distribution of the individual wheel forces using the quasi steady-state assumption is useful for the analysis of particular driveline configurations in relation to the combined lateral and longitudinal grip envelope [51, 55]. The addition of the QCLP problem formulation in this paper, makes another powerful tool available to the vehicle dynamics analyst to perform such studies.

4.3 Paper III – XWD Driveline Technology

This paper describes the development and vehicle integration of one particular all-wheel-drive driveline system, named XWD or cross-wheel-drive [27]. The XWD-system, shown in Figure 4.1, is comprised of an active on demand driven rear-axle, coupled to the front by means of an electronically controlled hydraulic clutch to distribute a variable amount of torque from front to rear. In addition to this front to rear distribution, the system is capable of transferring torque laterally across the rear-axle as well using an electronic limited slip differential (eLSD).

A complete system overview is provided in this paper, detailing each part of

the system and explaining both their mutual and external interfaces. Once having presented all key characteristics, the paper also presents how these characteristics determine system behavior on a vehicle level, i.e. especially on vehicle dynamics properties like traction and handling performance. Furthermore, the paper presents specific development implications related to the integration in the target application, i.e. how on one hand the vehicle architecture needed to be changed in order to incorporate the described system and how the system itself is tailored to excel in the particular vehicle.

4.4 Paper IV – Driver Warning Strategies

In this paper several indicators of instability are reviewed during a lane-change type maneuver. The lane-change type maneuver used here is the sine-with-dwell maneuver from the FMVSS-126 regulation [43]. The maneuver was suitable for our purpose of evaluating stability, since the maneuver is designed to invoke vehicle instability and thereby evaluating the ESC system's effectiveness to stabilize the vehicle.

It is assumed that it would be beneficial if the driver could cooperate with the ESC system by countersteering after the completion of the lane-change maneuver. For this purpose several indicators related to for instance the yaw acceleration and the side-slip rate together with a crude friction estimation were developed. These indicators are shown to give unambiguous warning thresholds on the two different surface for which these indicators were evaluated. These indicators, which were based on easily measurable variables, were further compared to classical evaluation tools such as the MMM diagram [38], phase portrait analysis and Lyapunov stability [26]. The conclusions are that stability indicators based on side-slip rate and yaw acceleration give an early indication of possible instability.

Other methods such as the Lyapunov analysis and deviation from a reference model gave an indication of instability only after completion of the maneuver. Additionally, the deviation from a reference model was used to trigger the ESC system which brakes the individual wheels to stabilize the vehicle.

It is shown in this paper that a combination of countersteer and ESC intervention triggered a quicker ESC intervention with a shorter duration. This is understood to show that a cooperation between the driver and the stability control gives a better overall system performance.

4.5 Paper V – Optimal Path Recovery Strategy

In this paper the problem of a vehicle overshooting a simple circular reference trajectory, due to friction limits, is considered. This is a situation referred to as terminal understeer [6] resulting from reaching the road holding limit of the front axle. In order to minimize the effects of a deviation from the desired trajectory, the path recovery task is formulated: to minimize the maximum off-tracking distance from the reference trajectory.

For any particular path recovery strategy, maximum off-tracking occurs when the direction of the velocity vector is tangent to the reference trajectory, provided the reference trajectory is sufficiently smooth and provided the vehicle speed at that instant no longer exceeds the maximum admissible tangential velocity for the future reference trajectory. In this work, the particular case of a circular reference trajectory was considered, and in this case a rigorous optimal control strategy was found for a particle model. It is found that minimum off-tracking is achieved by directing the force in a globally fixed direction, perpendicular to the path tangent at the anticipated point of maximum off-tracking. This recovery to the reference trajectory is identified as the well-known parabolic motion seen for ideal projectiles moving in free-fall under gravity. Because of the optimal path recovery being a projectile motion, the strategy is named the parabolic path recovery strategy.

It is further shown that the parabolic path recovery strategy can be successfully tracked by a model of rigid body motion of a passenger vehicle and can also be applied to non-circular reference trajectories. The parabolic path recovery is compared to a standard ESC understeer mitigation strategy based on braking the inner wheels. It is found that the new strategy solves the path recovery problem with significantly reduced off-tracking and better stability margins due to less side-slip.

Chapter 5

Discussion

This study covers a wide range of handling characteristics and the influence of longitudinal forces on these characteristics. In this chapter the main scientific contributions are summarized, conclusions are made and future work is identified.

5.1 Scientific Contributions

The main scientific contributions are presented in the appended papers. A summary of the most significant findings are given below.

In Paper I, a new axle-level combined friction model enables a correct representation of vehicles with open front and/or rear differentials using a simple single-track vehicle model relative to the commonly used more complex two-track vehicle model. This model represents the lateral load transfer due to cornering more accurately than a standard friction circle and much simpler than the two-track model.

In Paper II the objective is to develop a framework for the optimization of general driveline configurations for optimal combined grip. These problems have been addressed by using a simple load transfer model resulting in the quadratically constrained linear programming (QCLP) formulation. The QCLP formulation provides a faster and more flexible method to perform optimization of the wheel force distribution than methods currently available.

In Paper IV six different friction independent indicators of a critical cornering situation are evaluated. Two of these indicators are related to the Milliken Moment Method-diagram and one of them relates the stability of the vehicle to the Lyapunov stability. Since five of these indicators were able to identify the critical cornering situation approximately one-half to one second prior to the oversteer intervention from the ESC-system, these indicators could be used for driver warning

or activation of additional yaw damping from, for instance, an eLSD or TVD.

In Paper V the problem of path recovery is addressed for the case when the speed of a vehicle speed is too high to permit successful tracking of a circular reference path. The essential element of the presented approach is in the allocation of resultant vehicle forces derived from a simple particle representation. In this case the optimal path recovery is shown to be a classical parabolic trajectory resulting from a constant target acceleration vector. When this strategy is implemented for a simple vehicle model, the maximum deviation from the intended path is only half of that of a standard ESC understeer mitigation approach of braking the inner wheels.

5.2 Conclusions

This work sets out to improve the fundamental understanding of the driveline/vehicle system related to road-holding limit handling characteristics. This objective is achieved by introducing simplified mathematical models which, for instance, makes it possible to study the effects from front/rear drive force distribution using a simple single-track vehicle model. This is in contrast to the common approach of using a more complex two-track vehicle model for this purpose. Based on these models, closed form expressions that describe the influence of several common driveline configurations on the lateral grip, are developed.

Since much information can be conveyed in graphical representations, these were developed and extensively used in this study with actual driveline systems in mind. One example of this is the dynamic square method which is successfully applied to the analysis of actual vehicle applications as demonstrated in Papers I, II and III.

Having established the necessary modeling framework, these models have been used to optimize the longitudinal force distribution with the objective to maximize the combined longitudinal and lateral grip. In Paper I, where only the front and rear longitudinal force is varied the front/rear distribution that results in the maximum lateral grip could be graphically identified. For the case where also the left/right drive force distribution is varied, the new QCLP optimization problem formulation was applied to expand the work from Paper I. The strengths of the new QCLP formulation are that it is numerically efficient, and flexible in terms of configuration and direction into which the force vector is maximized. Apart from these benefits, the method is equally accurate as standard non-linear programming formulations currently available.

Although this study mainly focuses on longitudinal force distribution in driveline systems, the path recovery strategy shown in Paper V uses a brake force distribution based on a strategy which in Paper II is presented for a driveline sys-

tem. This demonstrates that much of the learnings developed for traction forces can also be extended to brake forces.

Dynamic stability is studied in Paper IV. As with the drive force optimization, a simple bicycle model is shown to be useful to explain the phenomena that create the yaw instability that is provoked by for instance the sine-with-dwell maneuver. For this purpose existing methods such as Lyapunov stability concepts and phase plane representations are applied in a new way to solutions that generate excessive yaw motion. The understanding of these fundamentals as presented in Paper IV mean that interventions from, for instance, an active differentials can be activated around one second prior to the intervention of an ESC-system and thereby expanding the range within which the driver remains in control of the vehicle.

The results obtained in this work can be applied for analysis of the performance of current and upcoming driveline and brake systems and as components in the associated active control for these systems. Overall, the present work has expanded the fundamental framework of vehicle modeling, optimization formulations and graphical representations for analysis and optimization of a wide range of driveline system properties and vehicle level characteristics.

5.3 Future Work

The findings in this project that considerable insight can be gained using simple models to better describe the limit handling characteristics during quasi steady-state conditions. Similar expansions can therefore likely be made to transient and dynamic effects from longitudinal force inputs. Theory describing the yaw damping effect from locked differentials as shown in Papers III, IV and V could for instance be expanded to limit handling conditions.

Further, of the four driveline configurations studied in Paper II, only for the fully active driveline, closed form expressions were derived that relate the drive force distribution to a given total drive force. A natural expansion in this area would be to find closed-form solutions also for other configurations. Another area for future research is to better understand the safety critical situations where longitudinal acceleration is vital to avoid an accident. It might be possible to solve some of these problems as an optimal control problem using a particle model in a similar fashion as is done in Paper V.

The methods developed in Paper IV for detecting a critical cornering situation require substantially more work before these methods could be implemented in a vehicle application, such as driver warning. More driving cases should be studied both to expand the detection capability of the system, but also to avoid false activations. The human/machine interface also requires a considerable amount of research and development as to the presentation of the warning and evaluation

of the driver's reaction to such a warning. Also other usages of early detection, not necessarily involving the driver such as earlier activation of yaw damping are indicated in the work and could be further explored.

It would also be interesting to study applications for the linear approximation of the quadratic tire constraints in Paper II. One likely application is model predictive control of similar problems as are studied in Paper V, but with a complete vehicle rather than only a particle representation.

Bibliography

[1] ABE, M., "A theoretical analysis on vehicle cornering behaviors in acceleration and in braking", in *9th IAVSD Symposium, Dynamics of Vehicles on Roads and on Tracks*, 1986.

[2] ABE, M., "Effects of traction force distribution control with additional rear wheel steer on turning behavior of 4wd vehicle", *Vehicle System Dynamics*, vol. 17, no. 6 supp 1, pp. 1–12, 1988.

[3] ABE, M., *Vehicle Handling Dynamics: Theory and Application*. Oxford: Butterworth Heinemann, 2009.

[4] ANDERSSON, M., BRUZELIUS, F., CASSELGREN, J., GÄFVERT, M., HJORT, M., HULTEN, J., HABRING, F., KLOMP, M., OLSSON, G., SJÖDAHL, M., SVENDENIUS, J., WOXNERYD, S., and WÄLIVAARA, B., "Road friction estimation", tech. rep., IVSS Project Report 2004:17750, 2007.

[5] ANDREASSON, J., *On Generic Road Vehicle Motion Modelling and Control*. PhD thesis, Royal Institute of Technology – Department of Aeronautical and Vehicle Engineering, 2006.

[6] BACKMARK, J., KARLSSON, E., FREDRIKSSON, J., and JONASSON, M., "Using future path information for improving the stability of an over-actuated vehicle", *International Journal of Vehicle Systems Modelling and Testing*, vol. 4:3, s. 218-231, 2009.

[7] BAKKER, E., NYBORG, L., and PACEJKA, H. B., "Tyre modelling for use in vehicle dynamics studies", in *SAE Technical Paper 870421*, 1987.

[8] BILLBERG, J., DOUHAN, A., and KLOMP, M., "Method and system for estimating a cornering limit of an automotive vehicle and a computer program

product for carrying out said method", in *Patent Application GB1001582.4*, 2010.

[9] DANESIN, D., GIRARDIN, C., SORNIOTTI, A., MORGANDO, A., and VELARDOCCHIA, M., "Driveline layout influence on four wheel drive dynamics", in *SAE Technical Paper 2004-01-0860*, 2004.

[10] DUKE, C., "Apollo 16 commander john young standing behind the lunar roving vehicle (lrv-2) at the descartes highlands with lunar module *Orion* (lm-11) in the background.", in *NASA Images AS16-117-18813 – 18819*, 1972.

[11] EDELMANN, J., PLÖCHL, M., LUGNER, P., MACK, W., and FALKNER, A., "Investigations on the powerslide of automobiles", in *Proceedings of the International Symposium on Advanced Vehicle Control (AVEC)*, 2008.

[12] FREDRIKSSON, J., *Nonlinear Model-based Control of Automotive Powertrains*. PhD thesis, Chalmers University of Technology, Department of Signals and Systems, 2002.

[13] GHONEIM, Y. A., LIN, W. C., LIN, W. C., and SIDLOSKY, D. M., "Enhanced traction stability control system", in *Journal of Passenger Car - Mechanical Systems*, (SAE International, Warrendale, Pennsylvania, USA), 2005. 2005-01-1591.

[14] GHONEIM, Y. A., LIN, W. C., SIDLOSKY, D. M., CHEN, H. H., CHIN, Y.-K., and TEDRAKE, M. J., "Integrated chassis control system to enhance vehicle stability", *International Journal of Vehicle Design*, vol. 23, pp. 124–144, 2000.

[15] GILLESPIE, T. D., *Fundamentals of Vehicle Dynamics*. SAE, 1992.

[16] HANCOCK, M., WILLIAMS, R., FINA, E., and BEST, M., "Yaw motion control via active differentials", *Transactions of the Institute of Measurement and Control*, vol. 29, no. 2, pp. 137–157, 2007.

[17] HORI, Y., "Future vehicle driven by electricity and control-research on four-wheel-motored "uot electric march ii"", *Industrial Electronics, IEEE Transactions on*, vol. 51, pp. 954–962, Oct. 2004.

[18] ISO TECHNICAL COMMITTEE TC 22/SC9, "Transient open-loop response test method with one period of sinusoidal input", in *ISO/TR 8725*, December 5 1988.

[19] ISO TECHNICAL COMMITTEE TC 22/SC9, "Vehicle dynamics and road-holding ability - vocabulary", in *ISO 8855*, 1991.

[20] ISO TECHNICAL COMMITTEE TC 22/SC9, "Lateral transient response test methods", in *ISO 7401*, 2003.

[21] ISO TECHNICAL COMMITTEE TC 22/SC9, "Steady-state circular driving behaviour", in *ISO 4138*, 2004.

[22] JONASSON, M., ANDREASSON, J., JACOBSON, B., and TRIGELL, A. S., "Global force potential of over-actuated vehicles", *Vehicle System Dynamics: International Journal of Vehicle Mechanics and Mobility*, vol. 99999, no. 1, pp. 1–16, 2010.

[23] JONASSON, M., *Exploiting individual wheel actuators to enhance vehicle dynamics and safety in electric vehicles*. PhD thesis, KTH, Aeronautics and Vehicle Engineering, 2009.

[24] KARNOPP, D., *Vehicle Stability*. Marcel Dekker, Inc., 270 Madison Avenue, New York, NY 10016, USA: CRC Press, 2004.

[25] KATO, M., ISODA, K., and YUASA, H., "Study on vehicle dynamics in marginal condition using dynamic square method", in *SAE Technical Paper 958503*, 1995. SAE-958503.

[26] KHAHIL, H., *Nonlinear Systems*. New Jersey: Prentice Hall, Third Edition ed., 2002.

[27] KLOMP, M., "Passenger car all-wheel drive systems analysis", Master's thesis, University West - Division of Mechanical Engineering, 2005.

[28] KLOMP, M., *On Drive Force Distribution and Road Vehicle Handling – A Study of Understeer and Lateral Grip*. Licentiate Thesis, Chalmers University of Technology, 2007.

[29] KLOMP, M., "Drive force distribution controlling method", in *Patent Application GB0821751.5*, 2008.

[30] KLOMP, M., "Drive mechanism for selectively switching a drive between propulsion and torque vectoring mode", in *Patent Application GB0900652.9*, 2009.

[31] KLOMP, M., "Method for judging track-keeping capacity of a vehicle", in *Patent EP 2 062 794 (A1)*, 2009.

[32] KLOMP, M. and DURINGHOF, H.-M., "Driveline and chassis of the Saab Turbo X", in *Vehicle Dynamics Expo – Open Technology Forum*, 2008.

[33] KLOMP, M. and THOMSON, R., "Influence of drive force distribution on the lateral grip and understeer", in *Proceedings of the 9th International Symposium on Advanced Vehicle Control*, 2008.

[34] KOBER, W. and RAMUSCH, F., "Fahrdynamikbeeinflussung durch kombinierten einsatz von hinterachsregelungssystemen", *VDI Berichte*, vol. 2014, pp. 49–63, 2007.

[35] LAINE, L., *Reconfigurable Motion Control Systems for Over-Actuated Road Vehicles*. PhD thesis, Chalmers University of Technology, Department of Applied Mechanics, 2007.

[36] LINDER, A., DUKIC, T., HJORT, M., MASTOMS, Y., MARDH, S., SUNDSTRÖM, J., VADEBY, A., WIKLUND, M., and ÖSTLUND, J., "Methods for the evaluation of traffic safety effects of antilock braking system (ABS) and electronic stability control (ESC) – a literature review", tech. rep., VTI report 580A, 2007.

[37] MILLIKEN, W. F., DEL' AMICO, F., and RICE, R. S., "The static directional stability and control of the automobile", in *SAE Technical Paper 760712*, 1976.

[38] MILLIKEN, W. F. and MILLIKEN, D. L., *Race Car Vehicle Dynamics*. SAE International, 1995. 1-56091-526-9.

[39] MIRZAEI, M., ALIZADEH, G., ESLAMIAN, M., and AZADI, S., "An optimal approach to non-linear control of vehicle yaw dynamics", *Proceedings of the Institution of Mechanical Engineers, Part I: Journal of Systems and Control Engineering*, vol. 222, no. 4, pp. 217–229, 2008.

[40] MOKHIAMAR, O. and ABE, M., "How the four wheels should share forces in an optimum cooperative chassis control", *Control Engineering Practice*, vol. 14, no. 3, pp. 295–304, 2006.

[41] MOTOYAMA, S., UKI, H., MANAGER, K. I., and MANAGER, H. Y., "Effect of traction force distribution control on vehicle dynamics", *Vehicle System Dynamics: International Journal of Vehicle Mechanics and Mobility*, vol. 22, no. 5, pp. 455–464, 1993.

[42] NHSTA, "Electronic stability control systems", tech. rep., FMVSS No. 126 – Final Regulatory Impact Analysis, 2007.

[43] NHSTA, "Laboratory test procedure for fmvss 126, electronic stability control systems", in *TP126-02*, 2008.

[44] ONO, E., HATTORI, Y., MURAGISHI, Y., and KOIBUCHI, K., "Vehicle dynamics integrated control for four-wheel-distributed steering and four-wheel-distributed traction/braking systems", *Vehicle System Dynamics*, vol. 44, pp. 139–151, February 2006.

[45] ONO, E., HOSOE, S., TUAN, H. D., and DOI, S., "Bifurcation in vehicle dynamics and robust front wheel steering control", *IEEE Transactions on Control Systems Technology*, vol. 6, pp. 412–420, 1998.

[46] OSBORN, R. P. and SHIM, T., "Independent control of all-wheel-drive torque distribution", *Vehicle Systems Dynamics*, vol. 44, pp. 529–546, July 2006.

[47] PACEJKA, H. B., "Simplified analysis of steady-state behaviour of motor vehicles", *Vehicle System Dynamics*, vol. 2, pp. 161–172, 173–183, 185–204, 1973.

[48] PACEJKA, H. B., *Tyre and Vehicle Dynamics*. Butterworth-Heinemann, Oxford, UK, 2nd ed., 2006.

[49] PARK, J., DUTKIEWICZ, J., and COOPER, K., "Simulation and control of dana's active limited-slip differential e-diff", in *SAE Technical Paper 2005-01-0409*, 2005.

[50] PARK, J. and KROPPE, W. J., "Dana torque vectoring differential dynamic trak", in *SAE Technical Paper 2004-01-2053*, 2004.

[51] PENG, H. and HU, J.-S., "Traction/braking force distribution for optimal longitudinal motion during curve following", *Vehicle System Dynamics*, vol. 26, no. 4, pp. 301–320, 1996.

[52] SAPRA, G., DAHLBERG, A., KLOMP, M., WOLRATH, C., and ULLMAN, M., "Clutch temperature model for early stages of development", in *Defensive Publication IPCOM000185624D*, 2009.

[53] SAPRA, G., DAHLBERG, A., KLOMP, M., WOLRATH, C., and ULLMAN, M., "Clutch temperature model for on-board measurement", in *Defensive Publication IPCOM000185625D*, 2009.

[54] SAWASE, K. and INOUE, K., "Maximum acceptable differential speed ratio of lateral torque-vectoring differentials for vehicles", *Proceedings of the*

Institution of Mechanical Engineers, Part D: Journal of Automobile Engineering, vol. 223, pp. 967–978, Aug. 2009.

[55] SAWASE, K. and USHIRODA, Y., "Improvement of vehicle dynamics by right-and-left torque vectoring system in various drivetrains", *Mitsubishi Technical Review*, vol. 20, pp. 14–20, 2008.

[56] SAWASE, K., USHIRODA, Y., and MIURA, T., "Left-right torque vectoring technology as the core of super all wheel control (s-awc)", *Mitsubishi Motors Technical Review*, vol. 18, pp. 16–23, 2006.

[57] SCHIEBAHN, M., ZEGELAAR, P., and HOFMANN, O., "Yaw torque control for vehicle dynamics systems – theoretical generation of additional yaw torque", *VDI-Berichte*, vol. 2014, pp. 101–119, 2007.

[58] SCHIEBAHN, M., ZEGELAAR, P., LAKEHAL-AYAT, M., and HOFMANN, O., "Analysis and coordination of multiple active systems for vehicle dynamics controls", in *Proceedings of the 9th International Symposium on Advanced Vehicle Control (AVEC)*, 2008.

[59] SCHMEITZ, A. J. C., BESSELINK, I. J. M., and JANSEN, S. T. H., "Tno mf-swift", *Vehicle System Dynamics*, vol. 45, no. 1 supp 1, pp. 121–137, 2007.

[60] SCHWARZ, R., DICK, W., MEISSNER, T., PINSCHMIDT, U., and MARTIN, F., "Dynamic steering and quattro with sport differential - two perfect partners for highest agility and active safety", in *FISITA World Automotive Congress*, 2008.

[61] SHIBAHATA, Y., ABE, M., SHIMADA, K., and FURUKAWA, Y., "Improvement on limit performance of vehicle motion by chassis control", *Vehicle System Dynamics*, vol. 23 (suppl), pp. 449–469, 1994.

[62] SNELSON, B., "1985 audi sport quattro s1. winner of the 1985 pikes peak international hill climb with michele mouton driving.", in *Wikimedia Commons*, 2006.

[63] SVENDENIUS, J., *Tire Modeling and Friction Estimation*. PhD thesis, Lund University, Department of Control, 2007.

[64] TOMARI, T., MORI, A., and SHIBAHATA, Y., "Development of sh-awd based on dyc (direct yaw control) concept", in *Proceedings of AVEC '06*, 2006.

[65] TSENG, H. E., ASHRAFI, B., MADAU, D., BROWN, T. A., and RECKE, D., "The development of vehicle stability control at ford", *IEEE/ASME Transactions on Mechatronics*, vol. 4, pp. 223–234, September 1999.

[66] VAN ZANTEN, A. T., "Bosch esp systems: 5 years of experience", in *SAE Technical Paper 2000-01-1633*, 2000.

[67] VELENIS, E., TSIOTRAS, P., and LU, J., "Optimality properties and driver input parameterization for trail-braking cornering", *European Journal of Control*, vol. 14, no. 4, pp. 308–320, 2008.

[68] VOSER, C., HINDIYEH, R. Y., and GERDES, J. C., "Analysis and control of high sideslip maneuvers", in *Proceedings of the International Symposium on Dynamics of Vehicles on Roads and Tracks*, 2009.

[69] WILLUMEIT, H.-P., NECULAU, M., VIKAS, A., and WÖHLER, A., "Mathematical models for the computation of vehicle dynamic behaviour during development", in *Proceedings of the 24th FISITA Congress*, 1992.

[70] YAMAMOTO, M., "Advice control strategy for improved handling and stability", in *SAE Technical Paper 911902*, 1991.